Supporting Information

Dynamic design: manipulation of millisecond timescale motions on the energy landscape of Cyclophilin A

Jordi Juárez-Jiménez[†*], Arun A. Gupta[†¬], Gogulan Karunanithy[$], Antonia S. J. S. Mey[†], Charis Georgiou[†¬], Harris Ioannidis[†], Alessio De Simone[†¬], Paul N. Barlow[†], Alison N. Hulme[†], Malcolm D. Walkinshaw[o], Andrew J. Baldwin[$] and Julien Michel[†*]

[†] EaStCHEM School of Chemistry, University of Edinburgh, David Brewster Road, Edinburgh, EH9 3FJ, United Kingdom.

[$] Department of Chemistry, Physical and Theoretical Chemistry Laboratory, University of Oxford, South Parks Road, Oxford, OX1 3QZ, United Kingdom.

[o] School of Biological Sciences, Michael Swann Building, MaxBorn Crescent, Edinburgh, EH9 3BF, United Kingdom.

[¬] Present Addresses: A. G: Department of Chemistry, University of Warwick, Coventry, CV4 7AL, United Kingdom; C.G: Department of Biomedicine, University of Bergen, 5020 Bergen, Norway; A.D.S: Sygnature discovery, Biocity, Nottingham NG1 1GR, United Kingdom.

[*] Corresponding authors. E-mail: jordi.juarez@ed.ac.uk, mail@julienmichel.net

Table of content

Supplementary Tables

Materials and Methods: Computational Methods

Accelerated Molecular Dynamics (aMD)

Initial exploration of the conformational landscape of CypA was performed by means of aMD[1,2] using the human Cyclophilin A structure from PDB ID: 1AK4[3] as starting point. Standard MD protein preparation procedures, including removal of co-crystallized proteins and co-solvent molecules and addition of missing hydrogen atoms, were followed. The protein was assigned ff14SB atom types and then solvated on an octahedral TIP3P[4] water box of 12 Å of radius and 1 Cl^- anion was added to neutralize the system. Prior to the aMD runs, the system was minimized combining 4500 steps of steepest descent followed by 7500 steps of conjugate gradient and subsequently heated from 100 K to 298 K in two stages of 125 ps (from 100 K to 200 K and from 200 K to 298 K) at constant volume. Density of the system was then equilibrated by means of a 250 ps long simulation at 298 K in the NPT ensemble. Throughout the heating and equilibration stages SHAKE[5] was applied to all bonds involving hydrogens and a time step 1 fs was employed. Finally, a conventional 100 ns simulation in the NVT ensemble, applying SHAKE to bonds involving hydrogen and using a 2 fs timestep, was performed.

During aMD runs, a positive energy boost is added to the potential energy function, therefore allowing for a simultaneous speed up in the sampling of multiple degrees of freedom without relying on a set of predefined collective variables. The boost potential ($\Delta V(\boldsymbol{r})$) is only applied when the average potential energy of the system ($V(\boldsymbol{r})$) falls below a certain threshold (E_P) and, therefore, the potential used in aMD simulations takes the form of eq 1.

$$V*(r) = \begin{cases} V(\boldsymbol{r}) & V(\boldsymbol{r}) > E_P \\ V(\boldsymbol{r}) + \Delta V(\boldsymbol{r}) & V(\boldsymbol{r}) < E_P \end{cases} \quad (1)$$

The current implementation of aMD in PMEMD[2] allows applying a dual boost approach where an energy boost is applied to all heavy atoms in the system and an additional boost is applied solely to the torsional degrees of freedom, hence the boost potential is given by eq 2.

$$\Delta V(\boldsymbol{r}) = \frac{(E_P - V(\boldsymbol{r}))^2}{(\alpha_P + E_P - V(\boldsymbol{r}))} + \frac{(E_D - V_D(\boldsymbol{r}))^2}{(\alpha_D + E_D - V_D(\boldsymbol{r}))} \quad (2)$$

where E_P and E_D are the reference potential and torsional energies respectively; V_D is the dihedral component of the potential energy and α_P and α_D serve to control the intensity of the boost applied to each term. Following guidelines of Pierce and co-workers[2], and the information obtained from the preliminary MD, a value of -81941 kcal/mol was used for E_P, while E_D was set to 2535 kcal/mol. After trial runs (data not shown), values of 2267 and 66 were used for α_P and α_D respectively. One common limitation of aMD is that a too intense energy boost may push the sampling towards high-energy regions of the Potential Energy Surface (PES), effectively triggering protein unfolding. To surpass this limitation harmonic restraints, using a force constant of 15 kcal mol^{-1} A^{-2}, were applied to the backbone atoms of residues that display α-helix or β-strand secondary structure in the crystallographic X-ray structure with PDB code 1AK4. At this stage, protein preparation was performed with tLeap and simulations were carried out employing the GPU accelerated version of PMEMD[6], both from the AMBER16[7] software package.

Molecular Dynamics (MD)

Structures sampled from the aMD trajectory were used as initial structures to seed sets of MD trajectories. Virtual sites were used in order to allow for a time step of 4 fs during MD simulations[8,9]. FF14SB atom types were assigned to the protein and each structure was then solvated in a 12 Å of radius dodecahedral water box and 1 Cl^- anion was added to neutralize

the system. Each system, comprising ca. 30000 atoms, was minimized combining 4500 iterations of steepest descent with 5000 iterations of conjugate gradient. Subsequently systems were heated from 0 K to 250 K in 150 ps in the canonical ensemble using a time step of 0.5 fs, and from 250 to 298 K in 300 ps using a timestep of 1 fs. Prior to the production runs each system was equilibrated for 300 ps at 298 K and 1 bar of pressure using 2 fs timestep, before switching to a 4 fs timestep for 10 ns under the same temperature and pressure conditions. Each system was then used for production runs consisting of 150 ns long trajectories in the NPT ensemble using a 4 fs timestep. using the leap-frog integrator and LINCS[10] algorithm was used to constrain bonds involving hydrogen, truncating the constraint coupling matrix at the sixth order. The generation of non-bonded pair lists was achieved with the Verlet scheme using a radius of 10 Å . Long range electrostatic interactions were handled using PME with a radius of 10 Å and a grid spacing of 1.6 Å and Van deer Waals interactions were handled using Lennard-Jones with a cut-off of 10 Å. The velocity rescaling coupling with a τ-t of 0.1 ps was used to control the temperature and pressure was controlled with the Parrinello-Rahman barostat with a τ-p of 2 ps. System compressibility was set at $4.5e^{-5}$ bar^{-1} and the selected reference pressure was 1.0 bar. Energy and pression corrections were employed to account for the Van deer Waals cut-off scheme. Default values were used for the remaining parameters and MD simulations were setup and conducted using the appropriate modules of the GROMACS5.0[11,12] software package.

MSM Generation

MSMs were built from the set of equilibrium MD trajectories using the pyEMMA 2.3.0 software package.[13] In order to achieve a successful dimensionality reduction for the MSM building movements of the 70s loop (spanning from residue 65 to 77) were accurately captured by the root mean square deviation of the loops Cα atoms with respect to their position in the X-ray structure 1AK4. However, the Cα RMSD of the 100's loop between

(spanning from Met100 to Ser110) failed to describe the flapping movement found by visual inspection of the trajectories, because significantly different snapshots were mapped to the same RMSD values. In order to accurately describe this movement the distance between the centre of mass (COM) of the 100s loop and the α-helix defined by residues Pro30 to Thr41 was simultaneously monitored. Subsequently, a negative value was assigned to those values of RMSD where such distance was shorter than in the X-ray structure (14 Å). The dimensionality of the MD trajectories was reduced by projecting onto these two RMSD based collective variables. K-means clustering using 100 clusters was used to obtain a microstate definition for the MSM construction. Different lagtimes were used to compute implied timescales of the dominant eigenvalues according to eq 3:

$$t_i = -\frac{\tau}{ln\,\lambda_i(\tau)} \qquad (3)$$

The resulting implied timescale (t_i) plots are shown in Figure S1. A Bayesian MSM was built at each lagtime (τ) in order to obtain an error estimate for the obtained timescales. Based on the implied timescales a lagtime of 40 ns was chosen for the MSM construction, with default parameters provided by PyEMMA.[14]

MSMs construction for the mutants was carried out using the same features for dimensionality reduction, and initial snapshots were obtained by re-using those from the CypA seeds, after mutation of appropriate residues. To facilitate comparative analyses the MSMs for CypA and the mutants were built on a common CV space and set of cluster centres obtained from clustering a combined set of 2000 MD trajectories (1200 for CypA and 400 for each mutant) amounting for a cumulative sampling time of ca. 260 μs.

MSM Coarse graining

Based on the eigenvalue structure of the transition matrix of the MSM, five macro-states were deemed useful for describing the slow dynamics of the system. The 100 k-means derived model was therefore coarse grained into 5 metastable conformations using a hidden Bayesian Markov Model.[15,16] This grouping successfully distinguished between ordered, disordered and intermediate states of the 70s-loop, but clustered together structures on both ends of the 100s loop CV range and did not allow for a direct comparison between CypA and D66A, due to the narrow separation of timescales in the mutant protein. A refinement of the coarse grained model was therefore achieved according to the following structural criteria: microstates with a value of the 100s loop CV below 4.5 Å and with a value of the 70s loop CV below 1.5 Å were assigned to the ground state (open/closed, orange). Microstates within the same cutoff of the 70s-loop CV but with values of the 100s-loop above 4.5 Å were assigned to the closed/closed metastable state (red). Microstates with values of the 70s-loop CV between 1.5 Å and below 4.0 Å were assigned to the intermediate macro-state (teal). Microstates with a a 100s-loop CV value < 4.5 Å and a 70s-loop CV value above 4.0 Å were assigned to the open/open state (magenta) while microstates with extreme values of the 100s-loop CV (>4.5 Å) and of the 70s-loop CV (>4.0 Å) were assigned to the closed/open (blue) macro-state. This structural assignment was found to be the one that best reproduced the hidden Bayesian Markov Model while allowing for direct comparison between CypA and mutant proteins. The robustness of the calculated assignment was asserted by recomputing the predicted populations of each macro-state whilst varying fractions of the total MD dataset (Figure S2). Mean first passage times (MFPTs) between pairs of non-adjacent macro-states states were computed as a weighted average of MFPTs over all pairs of microstates. MFPT between adjacent macro-states were computed between the two most populated microstates of each microstate.

Ensemble observables

Previously published structural ensembles: Comparison with experimental structural ensembles of CypA was performed by obtaining the NMR ensemble with PDB ID: 2N0T and the X-ray structure with PDB ID: 1AK4. The calculated ensemble for CypA was analysed by including all macrostates, or just the dominant macrostate (orange). This was done to determine how sensitive the observables are to the different loop conformations present in the ensemble.

NOEs and eNOEs: The distance between each of the 1253 atom pairs involved in eNOE signals and 2143 involved in NOE signals was calculated for each structure in the ensemble with MDTRAJ,[17] using CYANA definitions[18] for pseudo atoms representing non-distinguishable hydrogen atoms. Subsequently, a histogram weighted by the probability of each microstate of the MSM was built and the corresponding NOE signal between hydrogens *i* and *j* for each histogram was calculated as in equation (4):

$$r_{i,j}^{avg} = \langle r_{i,j}^{-6} \rangle^{\frac{-1}{6}} \qquad (4)$$

Each predicted signal was compared with the experimental value and for the eNOE signals it was considered fulfilled if the predicted value was within lower and upper limits ± a tolerance value of 0.5 Å. Standard NOE signals were considered fulfilled if the predicted value was below the upper limit derived from experiment. Errors were estimated by 1000 cycles of bootstrapping of the histograms from individual trajectories to generate ensemble histograms. The results are reported in Figure S3a.

Coupling Constants (^3J): Backbone ϕ/ψ dihedral angles were calculated with MDTRAJ for all the structures in the ensemble. Karplus[19,20] equations were used to obtain values for each type of ^{3}J and a histogram weighted by the probability of each microstate was subsequently

built. Error estimation was performed as for the prediction of NOE and eNOE. The results are reported in Figure S3b.

Residual Dipolar Couplings (RDCs): A representative set of 1000 snapshots gathered according to microstate probabilities of the Markov model was used to compute an average structure after removing translation and rotation movements. Subsequently, PALES[21] was used to calculate an alignment tensor that provided the best fit of experimental residual couplings for residues in the β-sheet and α-helix regions of CypA to this average structure using singular value decomposition.[22] A subset of 5000 structures of the conformational ensemble was used to compute average RDCs, and the corresponding Q value was calculated. For the MD ensemble an average weighted by the probability of each microstate was calculated, while for the NMR ensemble available in the literature an unweighted average over all structures was used. Errors on the average Q values were estimated by bootstrapping.

The Q factor considering only residues in helices and sheets is 0.23 indicating a good quality description of the overall fold by the MD simulations. This increases to 0.31 when flexible loops are also considered in the calculations. These figures are similar to those obtained for the X-ray structure of CypA. The poorer description of RDCs for residues in the flexible loops of CypA is not surprising considering the large amplitudes of backbone fluctuations. Zweckstetter, M. & Bax[23] have shown that a Q factor of ca. 0.35 corresponds to an average error in the alignment angle of 10 degrees. In addition the RDC back-calculation procedure from the MD ensemble used here is only rigorously valid for conformers in fast exchange, whereas the experimental data was measured for several loops residues that are in intermediate exchange. It is difficult to quantify the errors introduced by this approximation, but this may explain at least in part why the Q-factors for the flexible loops are larger than for the rigid regions.

To account for model errors caused by incomplete sampling and limited accuracy of the potential energy function used we also used the Bayesian Maximum Entropy reweighing tool BME to improve agreement with experimental data for the RDCs.[24] The procedure causes small changes in the populations of the 5 MSM macrostates (blue 0.08 —> 0.10; magenta 0.18 —> 0.09; orange 0.41 —.> 0.54; red 0.28 —> 0.24; teal 0.05 —> 0.01). These changes do not qualitatively affect the ranking of the macro states by populations, though overall the 70s closed states become more populated (ca. 70 to 90%). This leads to a Q-factor of the rigid regions of CypA is 0.20 and including the flexible loops the Q-factor is 0.21, thus the flexible loops are as well described as the rigid regions in the reweighted ensemble. Q-factor values of ca. 0.20 indicate that the structural description of the protein is of good quality.[25]

By comparison the Chi et al. NMR ensemble has a Q-factor of 0.36 for the rigid CypA regions and this increases to 0.37 when flexible loops are also considered. We also attempted to improve agreement against experimental data by reweighing the Chi et al ensemble with the software BME. In this case the best reweighed ensemble has a Q-factor of 0.31 (rigid regions only) and 0.30 (considering flexible loops as well). Camilloni et al. reported a global Q factor of 0.31 for a separate MD ensemble of CypA refined against chemical shifts.[26] Thus overall the present MD ensemble appears to more accurately account for the RDCs of the flexible loops than the other ensembles. A summary of these results is reported in Figure S3c.

Chemical shifts: For both CypA and D66A chemical shifts of backbone ^{15}N and ^{1}H nuclei for each microstate of the MSMs were estimated by sampling 100 snapshots from each microstate, and using ShiftX2[27] to calculate the average chemical shift value of each residue. The MSM transition probabilities were converted into a rate matrix and input to the software MultiEx together with the average chemical shift. MultiEx is an *N* site generalization of the *cpmg_compare* software that was previously written to simulate numerically CPMG for two site chemical exchange.[28] MultiEx takes as input chemical shift values for an *N* state system

and a rate matrix and provides simulated HSQC spectra that were used to produce the CSP plots. The chemical shifts of the NMR ensemble were computed assuming fast exchange between all structures in the ensemble. A summary of the overall results for WT CypA is given in Figure S3d.

Overall (Fig S3) the results for the above observables between the one macrostate and 5 macrostate ensemble are similar, indicating that these cannot reliably validate the existence of minor states in CypA and therefore that additional CPMG/R1p experiments are necessary to validate the proposed ensemble.

HetNOE values: A 2.5 μs MD simulation of CypA was initiated from a snapshots sampled from a well populated cluster of the MSMs of WT and D66A respectively. Snapshots were saved every 5 ps. The simulations were split in two separate trajectories of 1.25 μs each and analysed separately to estimate uncertainties in the calculated HetNOE values according to a protocol based on work from Robustelli et al.[29] Firstly N-H bond vector autocorrelation functions $C_{int}(t)$ were computed with eq 5 by aligning all snapshots to a reference structure to remove global tumbling motions with a maximum lag time τ of 100 ns.

$$C_{int}(t) = \langle P_2\,[\mu(t) \cdot \mu(t+\tau)]\rangle \qquad (5)$$

where $P_2[x]$ is the second Legendre polynomial of x, μ is the relevant bond vector scaled to unit magnitude, and angular brackets indicate averaging over time *t*. Ill-behaved $C_{int}(t)$ curves that showed no sign of converging towards a plateau region were discarded from further analyses. Next total autocorrelation functions were obtained by multiplying the $C_{int}(t)$ curves a global tumbling function $C_{glob}(t)$

$$C_{tot}(t) = C_{int}(t)C_{glob}(t) \qquad (6)$$

where $C_{glob}(t) = \exp(-t/\tau_g)$ with τ_g taken as the global tumbling time of WT and D66A, as determined from NMR relaxation measurements (9.1 ns and 9.2 ns respectively). Next orientational spectral density functions were calculated by discrete Fourier transform of the resulting simulated autocorrelation functions using eq 7

$$J(\omega) = \frac{2}{5}\mathrm{Re}\left[\int_{-\infty}^{+\infty} C_{tot}(t)e^{-i\omega t}dt\right] \quad (7)$$

Steady-state heteronuclear ^{1}H-^{15}N NOE values were determined with eq 8 that assumes only contribution from dipolar interactions:

$$HetNOE = 1 + \frac{\gamma_H}{\gamma_N}\frac{[6J(\omega_H+w_N)-J(\omega_H-\omega_N)]}{J(\omega_H-\omega_N)+3J(\omega_N)+6J(\omega_H+\omega_N)} \quad (8)$$

where γ_H and γ_N are the gyromagnetic ratios of hydrogen and nitrogen, and ω_H and ω_N are the proton and nitrogen resonance frequencies on a 600 MHz spectrometer for compatibility with the measurements carried out in this work. Uncertainties are reported as the standard error of the mean of the *HetNOE* values obtained from analysis of two separate 1.25 μs trajectories.

Materials and Methods: Experimental Methods

Expression Vectors

A wild-type $PPIA_{(1\text{-}165)}$ gene inserted downstream of an N-terminal hexa-histidine tag with one TEV protease cleavage site in pDEST™ 14 expression vector[30] was provided by the Edinburgh Protein Production Facility (EPPF). Site directed PPIA-D66A mutant gene construct was synthesized by GeneArt (ThermoFisher Scientific) and was subsequently subcloned into a modified pET-15b vector with N-terminal hexa-histidine tag and a thrombin protease cleavage site.

Protein Expression and Purification

Expression and purification CypA was achieved as previously described.[30] The D66A mutant clone construct was transformed into BL21(DE3)pLysS host cells and kept for incubation at 37°C in LB medium. Overnight grown bacterial cultures were induced with 1.0mM isopropyl-β-D-1-thiogalactopyranoside (IPTG) and then further incubated at 30°C for 4-6 hrs. Cells were harvested and lysed in phosphate buffer saline (P.B.S), pH 7.4 as lysis buffer using Constant Cell Systems Disruptor (1.1kW TS Benchtop) set at 25kpsi. The lysed fraction was centrifuged, and directly applied on a Ni^{2+}-affinity (GE Healthcare) column. Elution of fusion histidine tagged D66A was achieved with a step wise gradient of 20mM phosphate, 150mM NaCl, 500mM Imidazole, pH 7.4 buffer. Eluted fractions were concentrated and fusion protein sample was further kept for cleavage with thrombin protease at a 1:100 (w:w) protease:protein ratio at room temperature. The cleaved protein samples was further applied to a Ni^{2+}-affinity column and flow–thru protein fractions were collected with a loading buffer (20mM phosphate, 150mM NaCl, 30mM Imidazole, pH 7.4). The final protein purification was achieved by passing concentrated samples through a 16/60 Superdex75 size-exclusion chromatography (AKTA^{TM} pure, GE Healthcare) pre-equilibrated with 50mM phosphate, 1mM tris-(2-carboxyethyl) phosphine (TCEP), pH 6.5. ^{13}C,^{15}N uniformly enriched D66A protein was prepared by following the protocol described above using M9 minimal culture medium with (^{15}N) NH_4Cl as nitrogen source and D-($^{13}C_6$) glucose as carbon source as previously described.[31] The purity of unlabelled and labelled CypA and D66A samples was initially confirmed by SDS-PAGE and further by ESI-TOF mass spectrometric analysis. LC-MS profiles of unlabelled CypA and 15N-labelled D66A are shown in Fig S6 and Fig. S7 respectively.

NMR Methods

3D backbone assignment NMR experiments for the D66A mutated protein were performed on a Bruker Avance 800MHz spectrometer equipped with a cryogenic TCI probe at 25°C.

NMR sample consisted of 1.0mM of ^{13}C-,^{15}N-labelled D66A in 50mM phosphate, 1mM TCEP, (pH 6.5) and 10% D_2O (v/v). Backbone resonance assignment was achieved using the complementary set of experiments of HNCA and HN(CO)CA, HNCO and HN(CA)CO, CBCANH and CBCA(CO)NH.[32] Partial side chain resonances were assigned from the combined information content of ct-^{13}C HSQC and HBHA(CO)NH[32] spectra. All spectra were processed with the NMRPipe[33] and analysed using Sparky 3.1.[34] For automated sequence-specific NMR assignment, PINE-SPARKY[35] a probabilistic algorithm program was used. Secondary structure and backbone dihedral angles were predicted using TALOS+[36] using D66A chemical shifts assignment as input. A total 143 backbone residues out of 165 amino acids were assigned on D66A, excluding 6 prolines that could not be detected in ^{1}H-^{15}N HSQC spectra. Missing resonances for His70, Asn71, Thr73, Lys76 and Glu81 in D66A HSQC spectrum were attributed to the effect of the mutant on the backbone dynamics of the 70s-loop region. Chemical shifts for D66A have been deposited in BMRB (BMRB entry 12023).

Chemical Shift Changes.

The overall chemical shift changes ($\Delta\omega$) were determined using equation (9):

$$\Delta\omega = \sqrt{\left(5\Delta\,^{1}H\right)^{2} + \left(\Delta\,^{15}N\right)^{2}} \qquad (9)$$

Here, $\Delta^{1}H$ and $\Delta^{15}N$ are the changes in the proton and nitrogen dimensions, respectively. Figure S8 highlights some significant CSPs.

^{15}N NMR Relaxation Measurements

Backbone T1,T2 and {^{1}H}-^{15}N heteronuclear NOE (hetNOE) relaxation measurements were carried out with 1.0-1.3mM ^{15}N-labelled CypA and D66A using previously described pulse sequences[37]. The experiments were performed in an interleaved manner at field strengths of

500 and 600 MHz at 25°C. For T1 experiments, eight relaxation times were sampled from 100 ms to 1000 ms with a replicate point at 300 ms for error analysis. {^{1}H}-^{15}N heteronuclear NOE (hetNOE) relaxation measurements were recorded at both field strengths of 500 and 600 MHz using a water flip-back NOE pulse sequence run in an interleaved fashion with 5 s relaxation delay. For T_2 experiments, relaxation delays at eight different time points ranging from 20 to 150 ms with a replicate point at 20 ms were acquired. 2D datasets were processed using NMRpipe[33] and arrayed HSQC spectral cross peaks signal intensities as a function of variable time delays were fitted to single exponential decay using FuDa[38] to determine the R_1 and R_2 relaxation rates. HetNOE values were calculated by taking the ratio of peak intensities according to the equation I_{on}/I_{off} from experiments performed with and without ^{1}H pre-saturation. In total, 142 cross peaks for CypA and 149 cross peaks for D66A were used for analysis.

Model-free Analysis

Model-free analysis was performed using R_1, R_2 and hetNOE values for CypA and D66A with the relax software (d'Auvergne, Edward J. Gooley, Paul R., *Journal of Biomolecular NMR*, **2006**, *35*(2), 117-135). Residues identified as exchanging on the microsecond-millisecond time scale were excluded from analysis in determining the overall diffusion tensor. The globally fitted correlation times τ_c for both proteins are determined to be similar: 9.1 ns and 9.20 ns for CypA and D66A respectively. However, the analysis suggests that effective correlation times for internal motions of a large number of residues approaches that of the global tumbling time, and thus low values of generalized-order parameters may not reliably indicate fast motions (Figure S9).

^{15}N Backbone Relaxation Dispersion Experiments

Relaxation compensated ^{15}N backbone Carr-Purcell-Meiboom-Gill (CPMG) experiments[39] were carried out on 1.0-1.3mM ^{15}N-labelled wild-type CypA and D66A CypA variant protein samples. Data were collected at 10°C using magnetic field strengths of 500 and 600 MHz. The constant time relaxation delay was set to 32 ms. ^{15}N-relaxation dispersion profiles were generated from the cross-peak intensities obtained from the ^{1}H-^{15}N 2D datasets extracted for 14 values of the CPMG field strength, varying from 67 to 1000 Hz with two values of ν_{cpmg} acquired twice for error estimation in each dataset. Peak intensities as a function of CPMG frequency of ν_{cpmg} were quantified using FuDa.[38] Individual residue relaxation dispersion curves were evaluated for statistically significant dispersions for two-site exchange versus no exchange (flat horizontal line). Residues that displayed appreciable exchange contributions were identified and clustered for global analysis using the numerical simulation software CATIA[40], which fits k_{ex} and p_b globally and a $|\Delta\omega|$ for each exchanging residue. R_{Nz} and R_{HzNz} rates were measured for the proteins and used as inputs for CATIA to determine the differential relaxation rates of in-phase and anti-phase magnetization as well as the peak positions so that the effects of off-resonance pulses are fully accounted for. Off-resonance R1ρ relaxation dispersion experiments on ^{15}N were recorded on a 600 MHz field strength spectrometer at 10°C using the pulse sequence described by Korzhnev et. al.[41] (Fig S7) with offsets, $\Omega_0/2\pi$, ranging from -2.0 to 2.0 kHz, Ω_{ref} being the centre of the ^{15}N-spectrum (116.5 ppm) and a spin-lock field strength of 1040 Hz (see also Figure S10).

Isothermal Titration Calorimetry

Calorimetric experiments were carried out using an Auto-iTC200 micro-calorimeter (Malvern Instruments) at 25 °C. The titration experiments between compound i.e Ethyl n-[(4-

aminobenzyl)carbamoyl]glycinate and CypA and D66A protein samples were performed in 50mM phosphate, 1 mM Tris-(2-carboxyethyl) phosphine (TCEP) pH-6.5 buffer. In each experiment, the 200 µl sample cell was filled with 100 µM (CypA) or 200 µM (D66A) protein sample, and the 40 µl injection syringe with 2.0 mM or 5.0 mM compound solution. The titrations were performed with an initial 0.4 µl injection, followed by 19 injections of 2.0 µl at 240 s intervals, while stirring the solution at 750 rpm. Control experiments were also performed with compound titrated to carefully matched experimental buffer. Raw datasets were integrated and baseline corrected using NITPIC.[42] Binding constant, K_d values reported for compound versus CypA variants are results of titration experiments fitted with " A + B < -> AB' hetero-association model using the non-linear least square routine in-built within ITCsys and final single-site binding model results plotted with GUSSI.[42]

Crystallisation, Data Collection and Structure Determination

N-terminal hexa-histidine tag was removed from the purified D66A protein by incubation with Thrombin protease for 3 hours at room temperature. The protein was re-purified and concentrated to 25 mg ml^{-1} in X-ray buffer (20 mM Tris pH 7.4, 100 mM NaCl, 1 mM DTT). A stock solution of the reference compound at a concentration of 50 mM was prepared in X-ray buffer plus 25% v/v DMSO. The stock solution was mixed with protein solution at a 1:4 v:v ratio (ligand:protein) and equilibrated in ice for 30 minutes. The ammonium sulfate suite (QIAGEN) was then used to test the crystallisation of the complex. Crystals suitable for X-ray diffraction were grown by vapour diffusion using the sitting drop method at 17 ^{o}C. Drop consisted from 1:1 ratio of protein-ligand complex and well buffer and crystals were observed after one day in different well positions, including wells B7, D2, D8 and H5. Prior diffraction, crystals were cryoprotected by brief immersion in oil (1250 cSt from Sigma) and flash frozen in liquid nitrogen. X-ray diffraction data were collected at 100K at the Diamond Light Source synchrotron-radiation facility in Oxfordshire, England. Data were processed

with MOSFL [43] and AIMLESS [44]. Molecular replacement was used to solve the structure of D66A in complex with the reference ligand using PDB ID 4N1M. Structure refinement was performed using the Crystallographic Object-Oriented Toolkit (Coot) [45] and REMFAC5 software [46] part of the CCP4 suite [47].

Synthesis of Ethyl n-[(4-aminobenzyl)carbamoyl] glycinate (**1**)

Ligand **1** was synthesized applying a previously reported procedure.[48] Spectroscopic data confirmed the structure. The procedure is reported below:

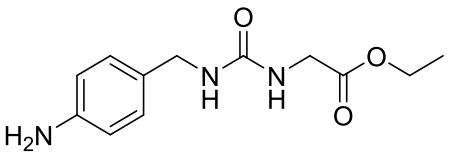

1

Ethyl isocyanatoacetate (0.4 mL, 3.68 mmol) was dissolved in DMF (15 mL). 4-Aminobenzylamine (0.4 mL, 3.68 mmol) was added and the reaction mixture was stirred at room temperature for 2 h. After this time, diethyl ether (50 mL) was added and the resultant solid was filtered off, yielding the desired product. White solid 900 mg (97% yield). ^{1}H NMR (500 MHz, DMSO-d_6) δ 6.94 – 6.88 (m, 2H), 6.53 – 6.47 (m, 2H), 6.39 (t, J = 5.8 Hz, 1H), 6.15 (t, J = 6.1 Hz, 1H), 4.92 (s, 2H), 4.09 (q, J = 7.1 Hz, 2H), 4.02 (d, J = 5.7 Hz, 2H), 3.77 (d, J = 6.0 Hz, 2H), 1.20 (t, J = 7.1 Hz, 3H). ^{13}C NMR (126 MHz, DMSO-d_6) δ 171.67, 158.30, 147.85, 128.51 (2C), 127.80, 114.13 (2C), 60.61, 43.20, 42.02, 14.59.

Supplementary Information References

1. Hamelberg, D., Mongan, J. & McCammon, J. A. Accelerated molecular dynamics: A promising and efficient simulation method for biomolecules. *J. Chem. Phys.* **120**, 11919–11929 (2004).

2. Pierce, L. C. T., Salomon-Ferrer, R., Augusto F. De Oliveira, C., McCammon, J. A. &

Walker, R. C. Routine access to millisecond time scale events with accelerated molecular dynamics. *J. Chem. Theory Comput.* **8**, 2997–3002 (2012).

3. Gamble, T. R. *et al*. Crystal structure of human cyclophilin A bound to the amino-terminal domain of HIV-1 capsid. *Cell* **87**, 1285–1294 (1996).

4. Price, D. J. & Brooks, C. L. A modified TIP3P water potential for simulation with Ewald summation. *J. Chem. Phys.* **121**, 10096–10103 (2004).

5. Miyamoto, S. & Kollman, P. A. SETTLE: an analytical version of the SHAKE and RATTLE algorithm for rigid water models. *J. Comput. Chem.* **13**, 952–962 (1992).

6. Salomon-Ferrer, R., Goetz, A. W., Poole, D., Le Grand, S. & Walker, R. C. Routine microsecond molecular dynamics simulations with AMBER on GPUs. 2. Explicit solvent particle mesh ewald. *J. Chem. Theory Comput.* **9**, 3878–3888 (2013).

7. Case, D. A. *et al*. Amber 16. *University of California, San Francisco* (2016). doi:10.1002/jcc.23031

8. Feenstra, K. A., Hess, B. & Berendsen, H. J. C. Improving efficiency of large time-scale molecular dynamics simulations of hydrogen-rich systems. *J. Comput. Chem.* **20**, 786–798 (1999).

9. Lindahl, E., Bjelkmar, P., Larsson, P., Cuendet, M. A. & Hess, B. Implementation of the charmm force field in GROMACS: Analysis of protein stability effects from correction maps, virtual interaction sites, and water models. *J. Chem. Theory Comput.* **6**, 459–466 (2010).

10. Hess, B. P-LINCS: A parallel linear constraint solver for molecular simulation. *J. Chem. Theory Comput.* **4**, 116–122 (2008).

11. van der Spoel, D. *et al*. GROMACS: Fast, Flexible and Free. *J. Comput. Chem.* **15**, 1701–1719 (2005).

12. Abraham, M. J. *et al*. GROMACS: High performance molecular simulations through multi-level parallelism from laptops to supercomputers. *SoftwareX* **1**–**2**, 19–25 (2015).

13. Scherer, M. K. *et al*. PyEMMA 2: A Software Package for Estimation, Validation, and Analysis of Markov Models. *J. Chem. Theory Comput.* **11**, 5525–5542 (2015).

14. Trendelkamp-Schroer, B., Wu, H., Paul, F. & Noé, F. Estimation and uncertainty of reversible Markov models. *J. Chem. Phys.* **143**, 174101 (2015).

15. Noé, F., Wu, H., Prinz, J. H. & Plattner, N. Projected and hidden Markov models for calculating kinetics and metastable states of complex molecules. *J. Chem. Phys.* **139**, 184114 (2013).

16. Chodera, J. D. *et al*. Bayesian hidden Markov model analysis of single-molecule force spectroscopy: Characterizing kinetics under measurement uncertainty. 1–12 (2011). doi:arXiv:1108.1430

17. McGibbon, R. T. *et al*. MDTraj: A Modern Open Library for the Analysis of Molecular Dynamics Trajectories. *Biophys. J.* **109**, 1528–1532 (2015).

18. Güntert, P. Automated NMR structure calculation with CYANA. *Methods Mol. Biol.* **278**, 353–378 (2004).

19. Karplus, M. Vicinal Proton Coupling in Nuclear Magnetic Resonance. *Journal of the American Chemical Society* **85**, 2870–2871 (1963).

20. Li, F., Lee, J. H., Grishaev, A., Ying, J. & Bax, A. High accuracy of Karplus equations for relating three-Bond J couplings to protein backbone torsion angles.

ChemPhysChem **16**, 572–578 (2015).

21. Zweckstetter, M. NMR: Prediction of molecular alignment from structure using the PALES software. *Nat. Protoc.* **3**, 679–690 (2008).

22. Chi, C. N., Strotz, D., Riek, R. & Vögeli, B. Extending the eNOE data set of large proteins by evaluation of NOEs with unresolved diagonals. *J. Biomol. NMR* **62**, 63–69 (2015).

23. Zweckstetter, M. & Bax, A. Evaluation of uncertainty in alignment tensors obtained from dipolar couplings. *J. Biomol. NMR* **23**, 127–137 (2002).

24. Bottaro, S., Bengtsen, T. & Lindorff-Larsen, K. Integrating Molecular Simulation and Experimental Data: A Bayesian/Maximum Entropy Reweighting Approach. *bioRxiv* (2018). doi:10.1101/457952

25. Chen, K. & Tjandra, N. The Use of Residual Dipolar Coupling in Studying Proteins by NMR. in *Topics in Current Chemistry* 47–67 (2011). doi:10.1007/128_2011_215

26. Camilloni, C. *et al*. Cyclophilin A catalyzes proline isomerization by an electrostatic handle mechanism. *Proc. Natl. Acad. Sci. U. S. A.* **111**, 10203–10208 (2014).

27. Han, B., Liu, Y., Ginzinger, S. W. & Wishart, D. S. SHIFTX2: Significantly improved protein chemical shift prediction. *J. Biomol. NMR* **50**, 43–57 (2011).

28. Baldwin, A. J. An exact solution for R2,eff in CPMG experiments in the case of two site chemical exchange. *J. Magn. Reson.* **244**, 114–124 (2014).

29. Robustelli, P., Trbovic, N., Friesner, R. A. & Palmer, A. G. Conformational dynamics of the partially disordered yeast transcription factor GCN4. *J. Chem. Theory Comput.* **9**, 5190–5200 (2013).

30. Wear, M. A., Nowicki, M. W., Blackburn, E. A., McNae, I. W. & Walkinshaw, M. D. Thermo-kinetic analysis space expansion for cyclophilin-ligand interactions – identification of a new nonpeptide inhibitor using Biacore™ T200. *FEBS Open Bio* **7**, 533–549 (2017).

31. Cai, M. *et al*. An efficient and cost-effective isotope labeling protocol for proteins expressed in Escherichia coli. *J. Biomol. NMR* **11**, 97–102 (1998).

32. Sattler, M., Schleucher, J. & Griesinger, C. Heteronuclear multidimensional NMR experiments for the structure determination of proteins in solution employing pulsed field gradients. *Prog. Nucl. Magn. Reson. Spectrosc.* **34**, 93–158 (1999).

33. Delaglio, F. *et al*. NMRPipe: A multidimensional spectral processing system based on UNIX pipes. *J. Biomol. NMR* **6**, 277–293 (1995).

34. Goddard, Td. & Kneller, D. G. Sparky 3. *Univ. California, San Fr.* **14**, 15 (2004).

35. Lee, W., Westler, W. M., Bahrami, A., Eghbalnia, H. R. & Markley, J. I. PINE-SPARKY: Graphical interface for evaluating automated probabilistic peak assignments in protein NMR spectroscopy. *Bioinformatics* **25**, 2085–2087 (2009).

36. Shen, Y., Delaglio, F., Cornilescu, G. & Bax, A. TALOS+: A hybrid method for predicting protein backbone torsion angles from NMR chemical shifts. *J. Biomol. NMR* **44**, 213–223 (2009).

37. Farrow, N. A. *et al*. Backbone dynamics of a free and phosphopeptide-complexed Src homology 2 domain studied by ^{15}N NMR relaxation. *Biochemistry* **33**, 5984–6003 (1994).

38. Hansen, D. F. *et al*. An exchange-free measure of ^{15}N transverse relaxation: An NMR

spectroscopy application to the study of a folding intermediate with pervasive chemical exchange. *J. Am. Chem. Soc.* **129**, (2007).

39. Loria, J. P., Rance, M. & Palmer, A. G. A Relaxation-Compensated Carr - Purcell - Meiboom - Gill Sequence for Characterizing Chemical Exchange by NMR Spectroscopy. *J. Am. Chem. Soc.* **121**, 2331–2332 (1999).

40. Hansen, D. F., Vallurupalli, P., Lundström, P., Neudecker, P. & Kay, L. E. Probing chemical shifts of invisible states of proteins with relaxation dispersion NMR spectroscopy: How well can we do? *J. Am. Chem. Soc.* **130**, 2667–2675 (2008).

41. Korzhnev, D. M., Skrynnikov, N. R., Millet, O., Torchia, D. A. & Kay, L. E. An NMR experiment for the accurate measurement of heteronuclear spin-lock relaxation rates. *J. Am. Chem. Soc.* **124**, 10743–10753 (2002).

42. Brautigam, C. A., Zhao, H., Vargas, C., Keller, S. & Schuck, P. Integration and global analysis of isothermal titration calorimetry data for studying macromolecular interactions. *Nat. Protoc.* **11**, 882–894 (2016).

43. Battye, T. G. G., Kontogiannis, L., Johnson, O., Powell, H. R. & Leslie, A. G. W. iMOSFLM: A new graphical interface for diffraction-image processing with MOSFLM. *Acta Crystallogr. Sect. D Biol. Crystallogr.* **67**, 271–281 (2011).

44. Evans, P. R. & Murshudov, G. N. How good are my data and what is the resolution? *Acta Crystallogr. Sect. D Biol. Crystallogr.* **69**, 1204–1214 (2013).

45. Emsley, P., Lohkamp, B., Scott, W. G. & Cowtan, K. Features and development of Coot. *Acta Crystallogr. Sect. D Biol. Crystallogr.* **66**, 486–501 (2010).

46. Murshudov, G. N. *et al.* REFMAC5 for the refinement of macromolecular crystal

structures. *Acta Crystallogr. Sect. D Biol. Crystallogr.* **67**, 355–367 (2011).

47. Winn, M. D. *et al*. Overview of the CCP4 suite and current developments. *Acta Crystallographica Section D: Biological Crystallography* **67**, 235–242 (2011).

48. Shore, E. R. *et al*. Small Molecule Inhibitors of Cyclophilin D to Protect Mitochondrial Function as a Potential Treatment for Acute Pancreatitis. *J. Med. Chem.* **59**, 2596–2611 (2016).

49. Schwarzinger, S., Kroon, G. J. A., Foss, T. R., Wright, P. E. & Dyson, H. J. Random coil chemical shifts in acidic 8 M urea: Implementation of random coil shift data in NMRView. *J. Biomol. NMR* (2000). doi:10.1023/A:1008386816521

50. Ke, H. Similarities and differences between human cyclophilin A and other β-barrel structures. *J. Mol. Biol.* **228**, 539–550 (1992).

Supplementary Figures

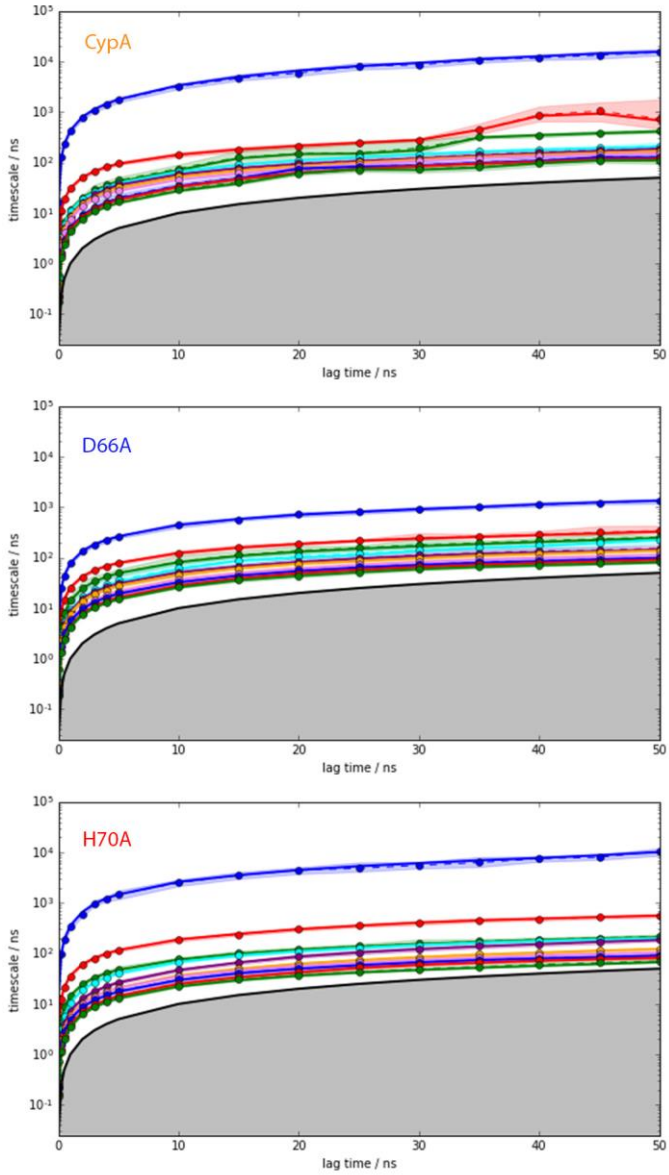

Figure S1: Implied timescales of the predicted MSM as a function of lagtime. Shaded region represents the estimated statistical errors.

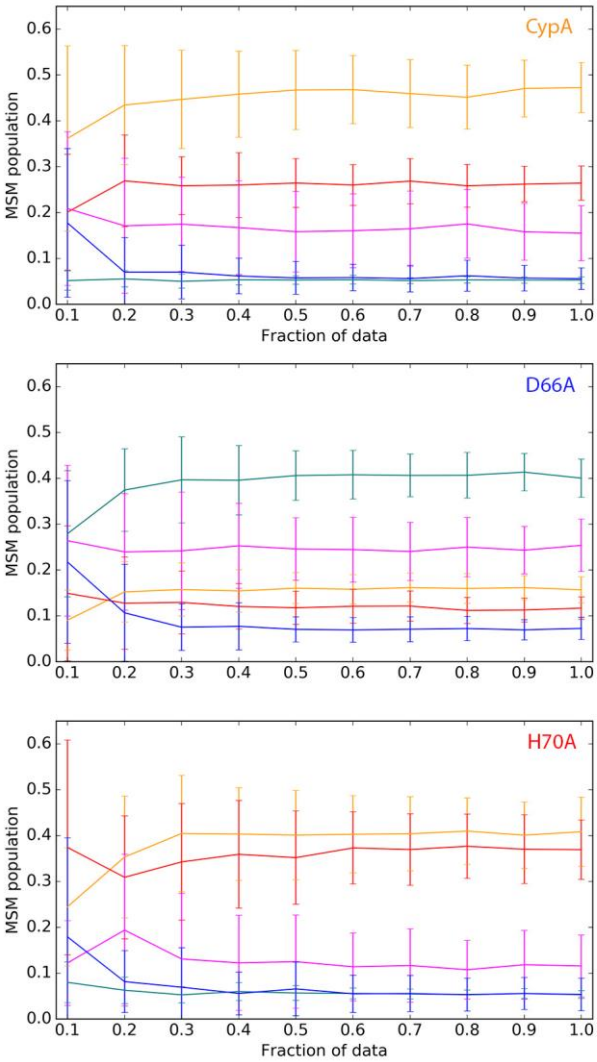

Figure S2: Predicted population of each MSM macrostate as a function of the fraction of the total dataset used to build the model. Error bars were obtained by bootstrapping.

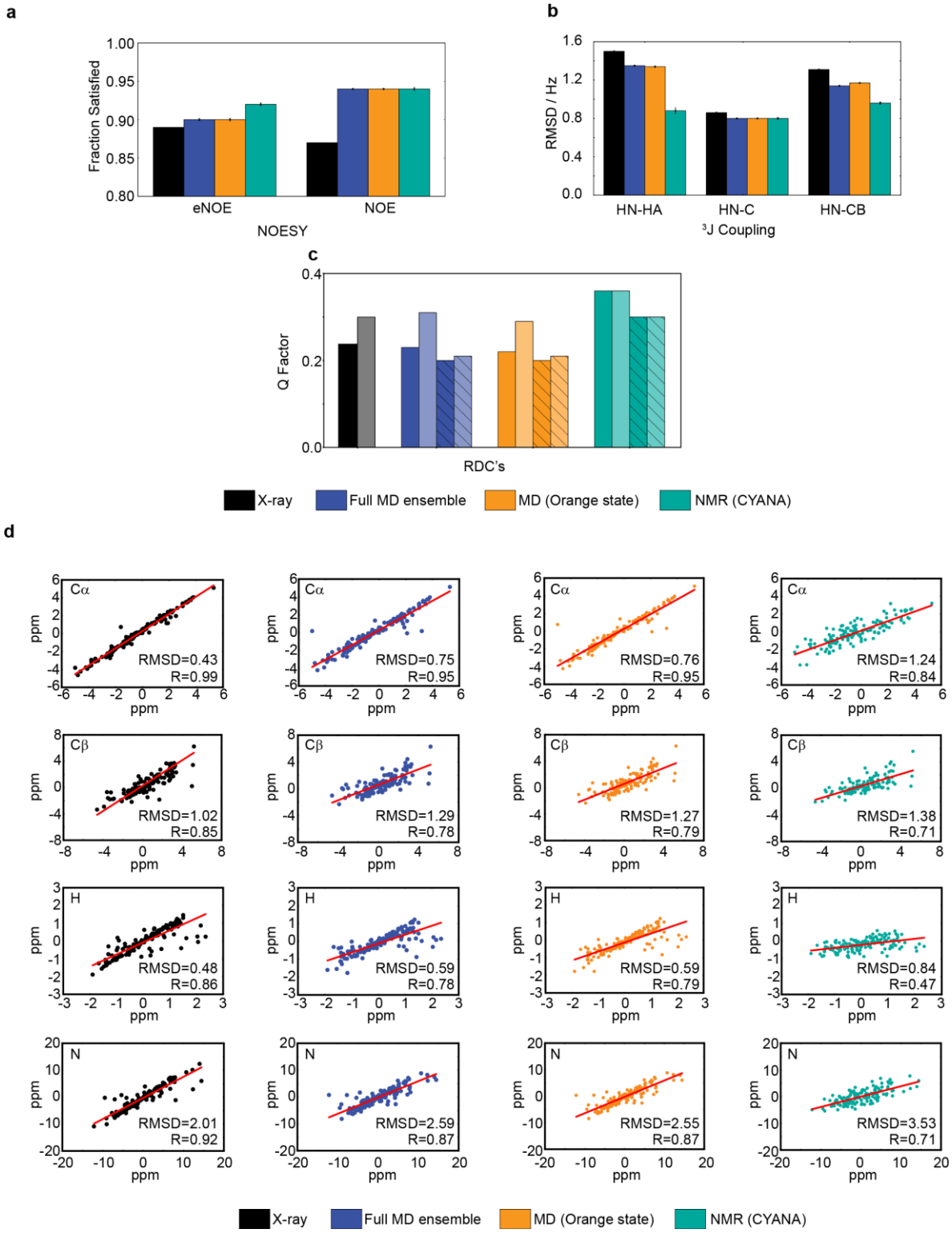

Figure S3. Calculated observables for the X-ray structure, MD and NMR ensembles of CypA. **a NOEs**. The MD ensembles reproduce the vast majority of eNOE and NOE-derived protein proton distances. The NMR ensemble was refined against this set of NOEs but shows almost identical accuracy. The X-ray structure is the least consistent with the NOE data. **b J-couplings**. The NMR

ensemble is more accurate at reproducing HN-HA and HN-HN couplings and of similar accuracy to the MD ensembles for HN-C couplings. This may be because the ensemble was refined against this set of observables. The X-ray structure is the least consistent with the J-couplings data. **c RDCs**. Dark bars correspond to secondary structure regions, whereas light bars also include the flexible loops. Shaded bars correspond to results obtained with reweighting. See SI text for a detailed discussion. The NMR ensemble is less accurate than the MD ensembles at reproducing RDCs. This may be because the NMR ensemble was not refined against this particular set of RDCs that come from a separate study.[26] **d** Correlation plot of experimental and predicted values of backbone N, H, C_α and C_β secondary chemical shifts. Random coil values were taken from Schwarzinger *et. al.*[49] The best results are obtained using the crystal structure of CypA, but this may be fortuitous as CypA was included in the training set of crystal structures used to calibrate ShiftX2.[27,50]

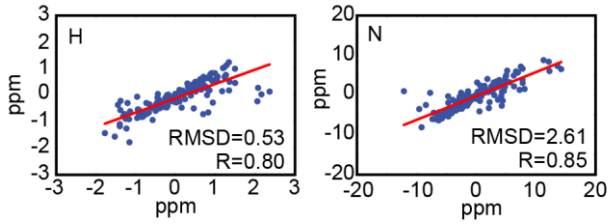

Figure S4. Correlation plot of experimental and predicted values of backbone N, H, secondary chemical shifts for the D66A CypA. Details as in figure S3.

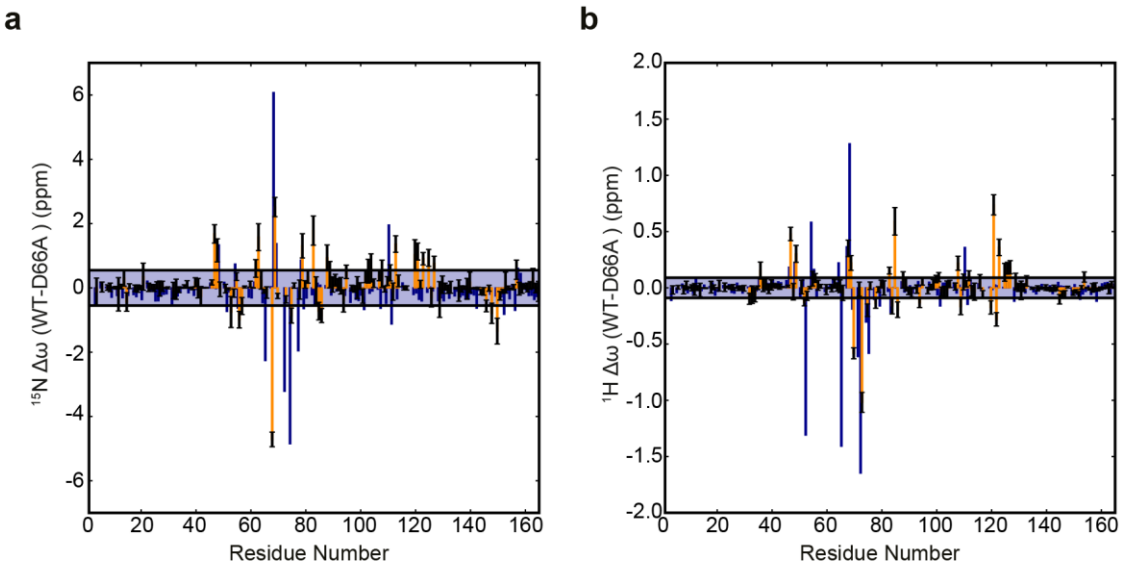

Figure S5. a. Measured (blue) and computed (orange) per residue WT-D66 ^{15}N Δω. Shaded area represents ± ½ of the Shiftx2 RMSD reported in the literature for the ^{15}N nuclei. **b** Measured (blue) and predicted (orange) per residue WT-D66 ^{1}H Δω. Shaded area represents ± ½ of the Shiftx2 RMSD reported in the literature for the ^{1}H nuclei. Several factors, including the accuracy of the predictor, inaccuracies inherent to the forcefield and finite sampling errors preclude a one to one agreement in the prediction of Δω. In particular many residues show Δω values that fall within the expected accuracy of ShiftX2. Considering only residues with observed Δω above ±½ of the Shiftx2 RMSD for each nuclei yields correlation coefficients of 0.76 and 0.61 for the 15N and 1H respectively, indicating qualitative agreement between experiment and simulation.

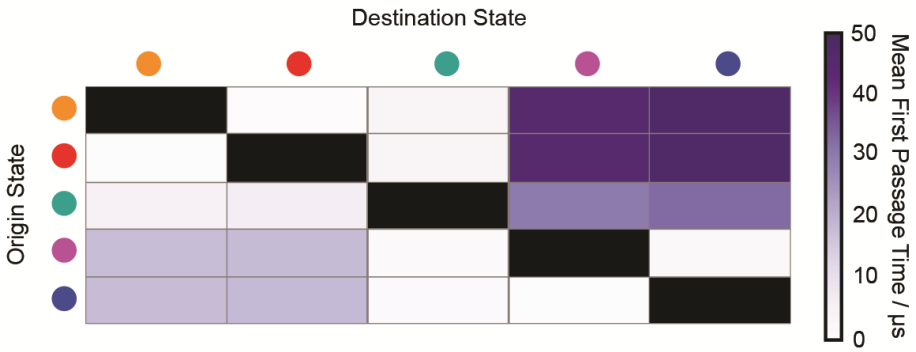

Figure S6. Mean First Passage Time among CypA MSM macrostates. Transitions involving the 70s loop disordering is approximately one order of magnitude slower than transitions involving 100s loop flapping.

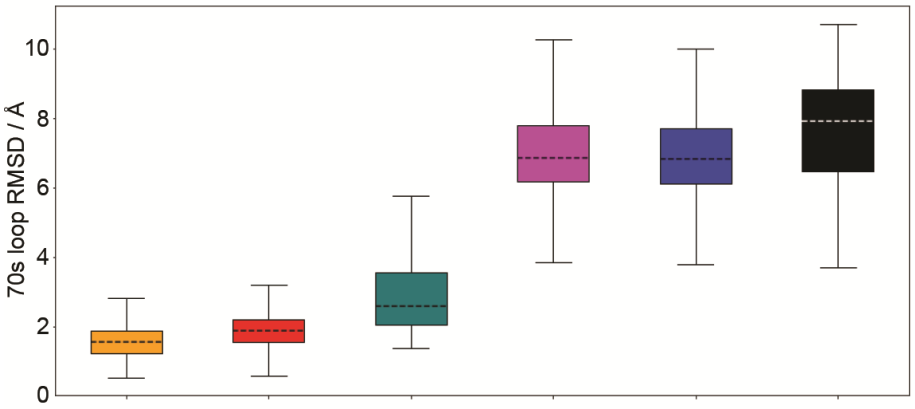

Figure S7. Per state boxplot of RMSD values of the 70s loop with respect to reference X-ray structure 1AK4. Each color identifies a macrostate as described in the main text and the 2N0T NMR bundle is shown in black.

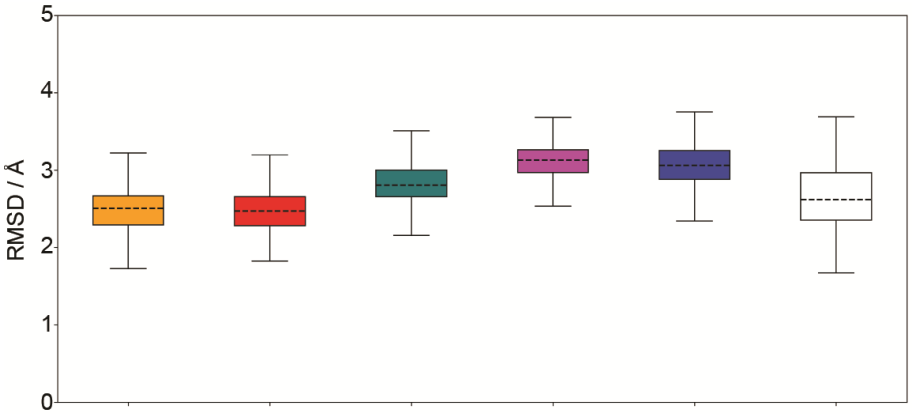

Figure S8. Per state boxplot of RMSD values of all atoms excluding the 70s and 100s loops with respect to reference X-ray structure 1AK4. Each color identifies a macrostate as described in the main text and the complete ensemble is shown in white. Considering estimated uncertainties no significant differences were identified among macrostates.

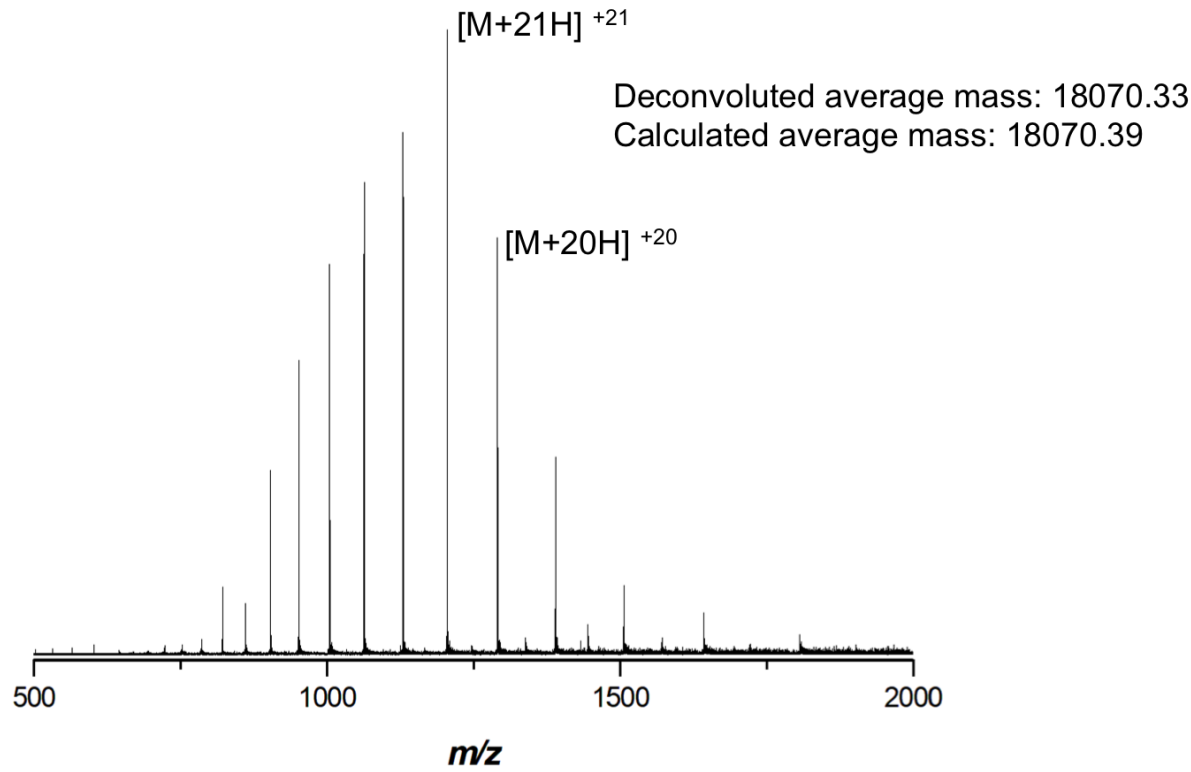

Figure S9. Positive mode mass spectrum acquired by LC-MS of wt-CypA following cleavage. A charge state distribution can be seen, and the $[M+21H]^{+21}$ and $[M+20H]^{+20}$ ions have been highlighted. The deconvoluted average mass was calculated to be 18070.33 Da, in agreement with the calculated theoretical average mass of 18070.39 Da.

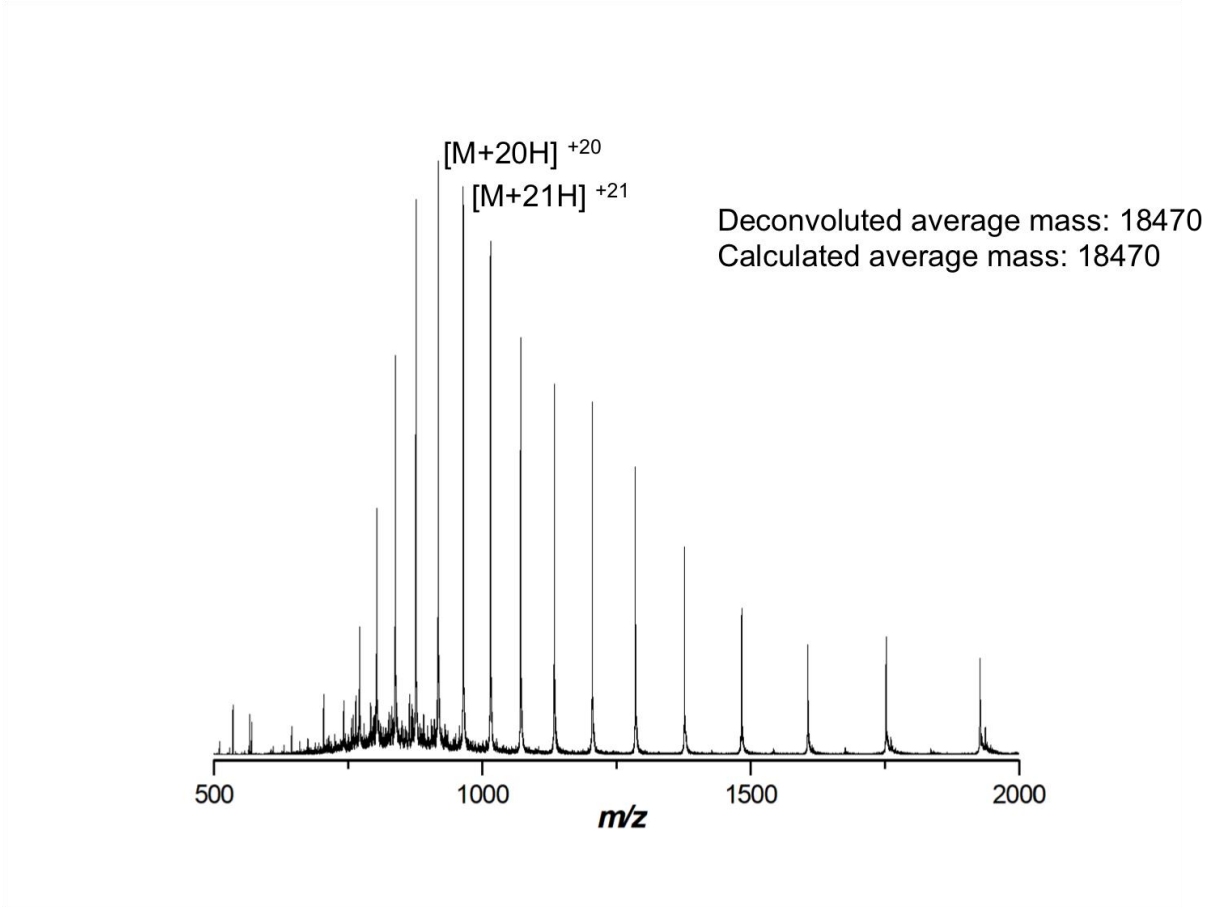

Figure S10. Positive mode mass spectrum acquired by LC-MS of ^{15}N labelled D66A CypA following cleavage. A charge state distribution can be seen, and the $[M+21H]^{+21}$ and $[M+20H]^{+20}$ ions have been highlighted. The deconvoluted average mass was calculated to be 18470 Da, in agreement with the calculated theoretical average mass of 18470 Da.

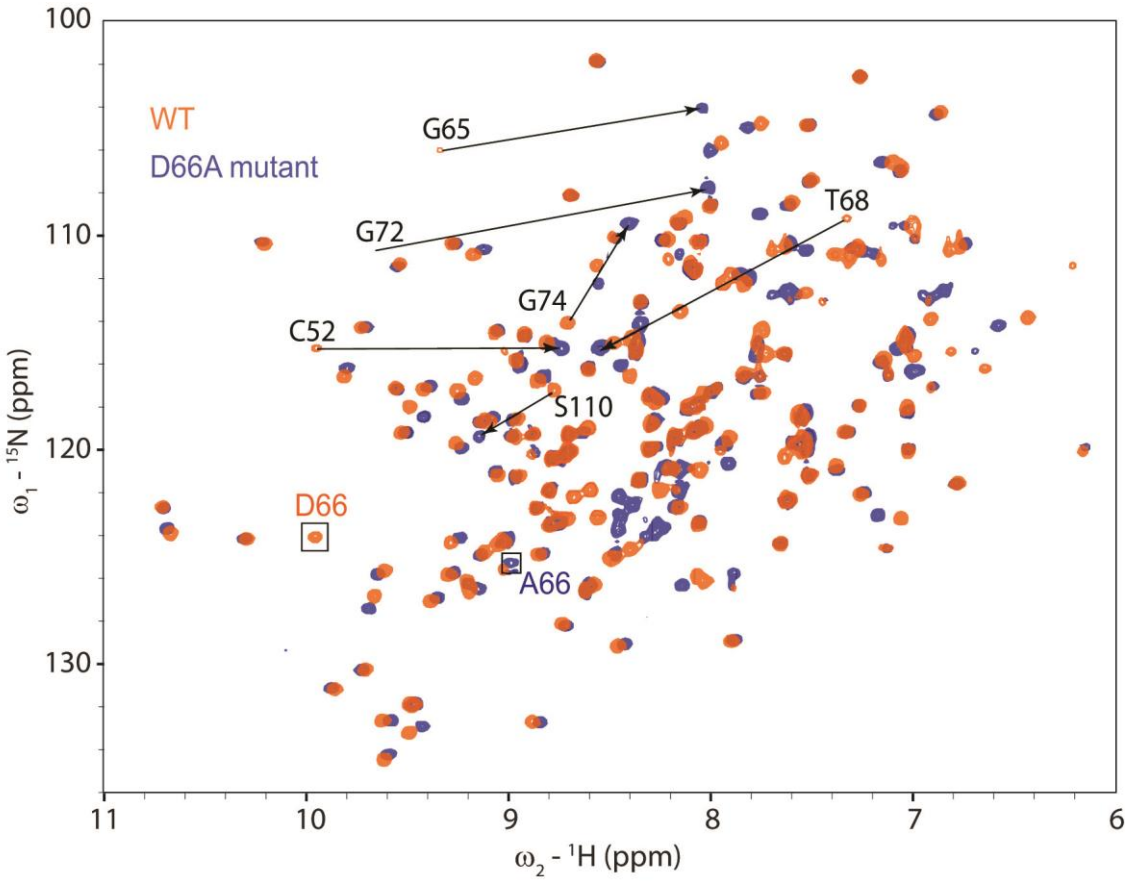

Figure S11. Comparison of CypA WT and D66A ^{15}N-^{1}H HSQC spectra with several residues showing large chemical shift perturbations (CSPs) highlighted. Most of these large CSPs occur in the 70s and 100s loops, showing a large difference in the ground state structure of the two proteins in this area.

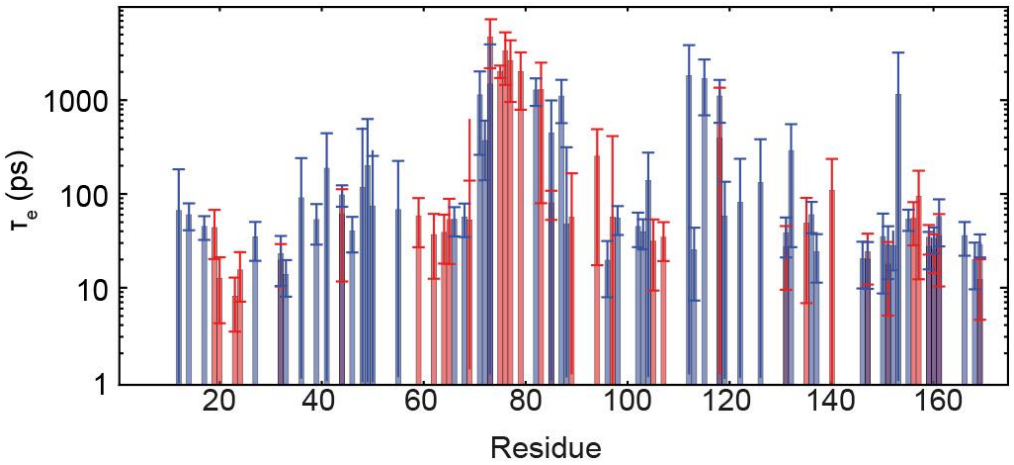

Figure S12. Using the relaxation data, a model-free analysis was carried out using the software package relax. t_e is the effective correlation time for internal motion. Red denotes data for CypA and blue data for D66A. For residues in the 60 to 90 region the model free treatment fits t_e values which approach the global tumbling time, and thus low values of generalized-order parameters derived from the model-free analysis are not indicative of fast motions.

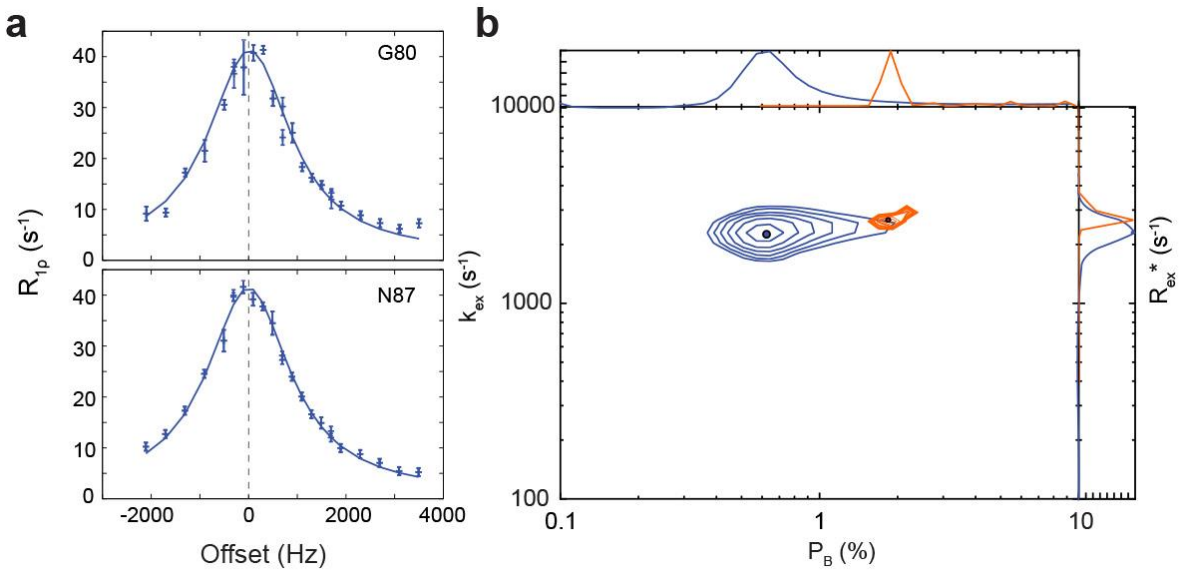

Figure S13 a. In addition to CPMG relaxation-dispersion, $R_{1\rho}$ experiments were carried out on the mutant protein as CPMG alone was insufficient to characterise exchange its parameters. By fitting the R1ρ data simultaneously with the CPMG dispersion profiles we could characterize the chemical exchange more precisely and also determine the signs for the chemical shift differences between the ground and excited state. **b.** Results of grid searching errors for fits of relaxation-dispersion data from the WT and D66A mutant. In both cases we find that we can fit the data well using a single p_b and k_{ex} for each protein. As seen in the results while the best fits of k_{ex} are similar in both cases the population of the excited state in the mutant is significantly lower. It should be noted however that the 'excited' state appears to be different for the two proteins.

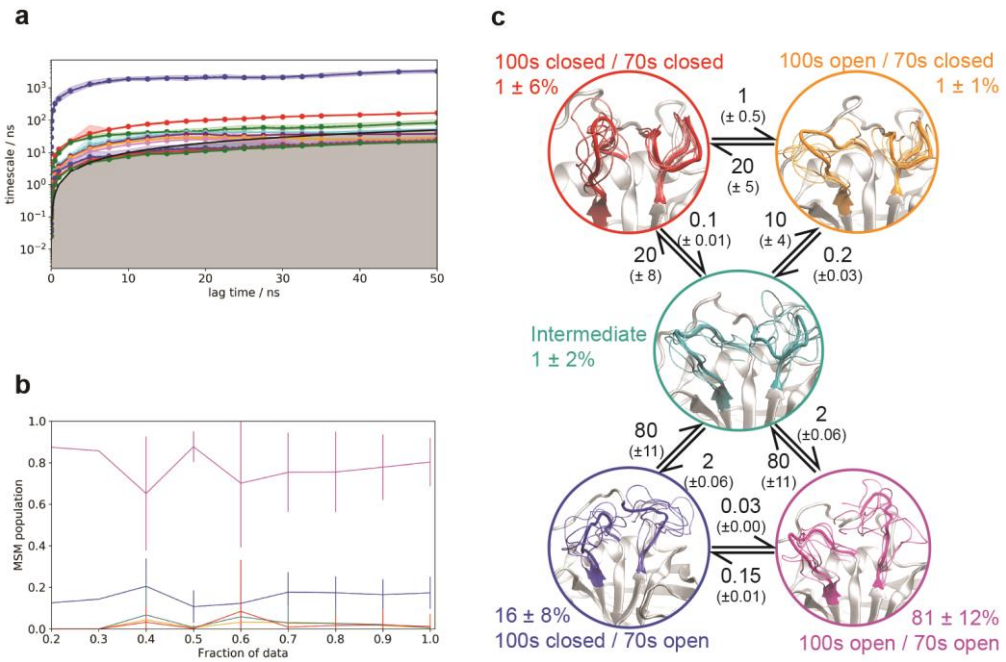

Figure S14. a Implied timescales of the MSM derived from the aMD trajectories as a function of lagtime. Shaded region represents the error as estimated by Bayesian analysis. **b** Predicted population of each MSM macrostate as a function of the fraction of the total dataset used to build the model. **c** Minimal set of sub-states that together contain the relevant amplitudes of motion and time-scales of state-to-state inter-conversion present in the full ensemble. The calculated rates and populations are indicated. Error bars on reported populations were obtained by bootstrapping of the MD trajectories assigned to the individual microstates.

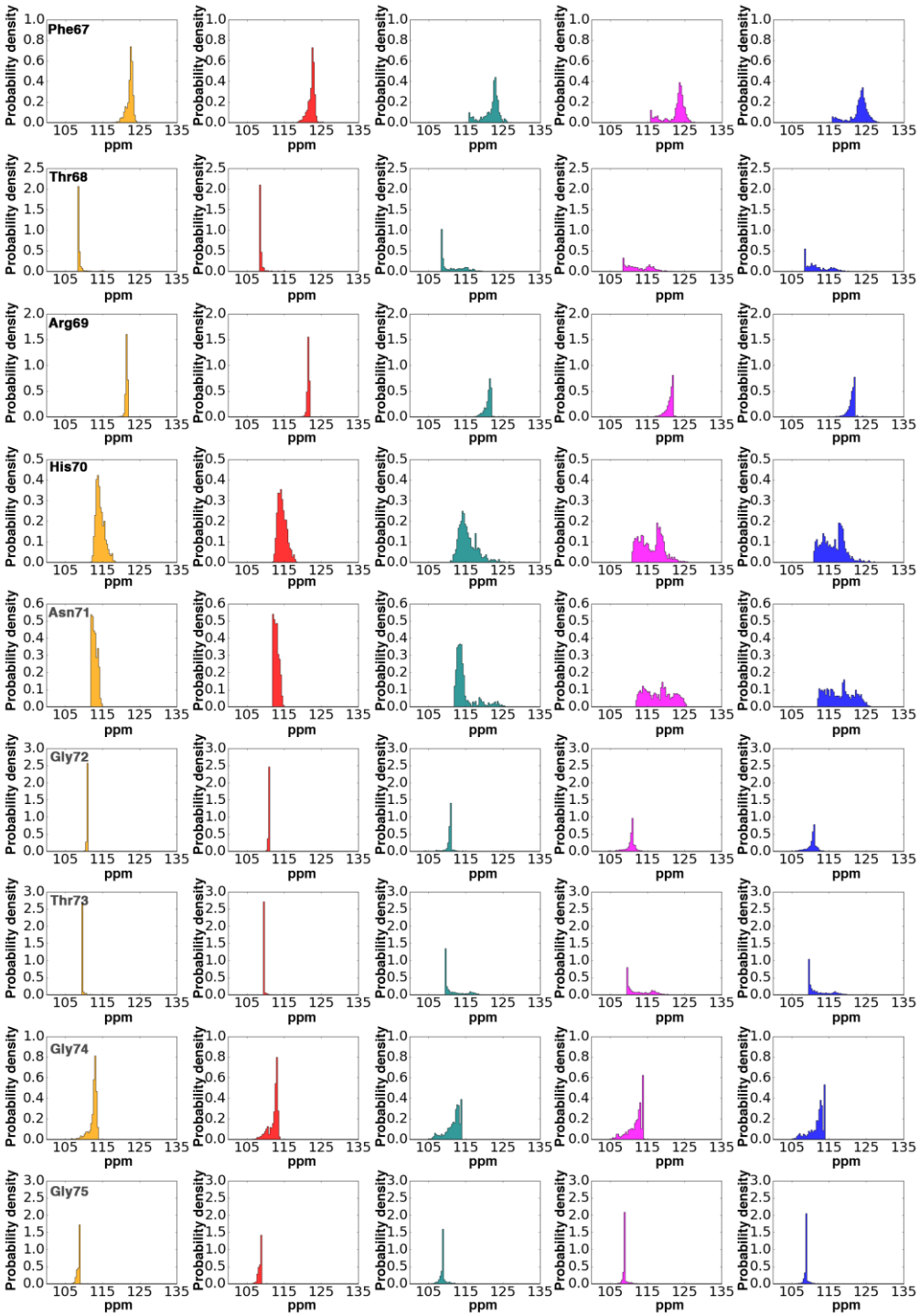

Figure S15. Distribution of calculated ^{15}N chemical shift values per macrostate for residues in the 70s loop region.

Supplementary Tables

Table S1. NMR assigment of CypA kindly provided by Dr. Xavier Hanoulle and Prof. Guy Lippens.

	Chemical shift (ppm)							
Residue	**H^N**	**H^α**	**H^β**	**other ^1H**	**^{15}N**	**$^{13}C^\alpha$**	**$^{13}C^\beta$**	**other ^{13}C, ^{15}N**
Met 1		4.12	2.14	H^γ 2.58, 2.54; H^ε 2.09		54.8	32.9	C^γ 30.7; C^ε 16.7
Val 2		4.19	2.05	H^γ *0.94, 0.93*		61.5	33.1	C^γ *20.8, 20.2*
Asn 3	8.64	5.14	*2.77, 3.62*	$H^{\delta2}$ 8.45, 6.98	126.5	51	37.7	$N^{\delta2}$ 109.7
Pro 4		4.75	*1.71, 2.36*	H^γ *2.09, 2.19*; H^δ 4.09, 4.06		62.7	33	C^γ 26.7; C^δ 50.6
Thr 5	8.76	5.72	4.05	$H^{\gamma2}$ 1.20	114.8	60.6	70.7	C^γ 22.1
Val 6	8.75	5.34	2.3	H^γ *1.05, 1.07*	120.1	58.7	36.1	C^γ *21.7, 20.6*
Phe 7	8.95	5.89	2.84, 2.63	H^δ 6.73; H^ε 6.99; H^ζ 7.06	119	55.7	43	C^δ 132.0; C^ε 130.5; C^ζ 129.5
Phe 8	9.53	5.32	*3.46, 3.25*	H^δ 7.49; H^ε 7.18; H^ζ 6.19	116.8	53.3	42.8	C^δ 129.1; C^ε 131.1; C^ζ 130.5
Asp 9	9.26	5.53	2.85, 2.52		124	54.7	41.2	
Ile 10	9.02	5.17	2.06	$H^{\gamma1}$ 1.84, 1.66; $H^{\gamma2}$ 0.96; H^δ 0.99	124.1	58.1	37.6	$C^{\gamma1}$ 27.0; $C^{\gamma2}$ 18.4; $C^{\delta1}$ 11.4
Ala 11	9.6	5.17	1.05		132.2	50.7	22.6	
Val 12	8.93	4.51	1.78	H^γ *0.34, 0.65*	118.2	60.3	33.1	C^γ *21.1, 21.6*
Asp 13	9.83	4.31	3.09, 2.50		130.7	55.5	39.8	
Gly 14	8.54	4.21, 3.42			101.5	45.1		
Glu 15	8.03	4.84	2.09, 1.98	H^γ 2.29, 2.19	123	52.8	30.2	C^γ 35.5
Pro 16		4.18	*1.88, 2.32*	H^γ 2.15, 1.98; H^δ 3.95, 3.72		64.5	32.2	C^γ 27.5; C^δ 50.9
Leu 17	9.18	4.69	1.60, 1.41	H^γ 1.56; H^δ *0.98, 0.82*	125.8	55.3	44.1	C^γ 27.4; C^δ *22.6, 25.7*
Gly 18	7.24	4.26, 3.95			102.2	45		
Arg 19	8.32	5.62	1.99, 1.62	H^γ 1.61, 1.47; H^δ 2.77, 2.67; H^ε 9.01; H^η 6.09	121	54.9	33.3	C^γ 26.9; C^δ 43.0; N^ε 85.9; N^η 70.4
Val 20	9.36	4.6	1.74	H^γ *0.51, 0.85*	126.6	59.9	34.8	C^γ *22.3, 21.9*
Ser 21	8.75	5.51	3.72, 3.56		120.1	55.2	66.3	
Phe 22	9.51	5.24	*2.30, 2.43*	H^δ 6.52; H^ε 6.15; H^ζ 6.64	118.9	55.7	42.5	C^δ 131.9; C^ε 130.4; C^ζ 128.3
Glu 23	8.74	4.75	1.82, 1.68	H^γ 2.19, 1.80	122.9	54.9	31.6	C^γ 36.5
Leu 24	8.18	4.7	*1.88, 1.23*	H^γ 1.69; H^δ *1.10, 0.46*	122.3	51.6	43.1	C^γ 26.9; C^δ *26.7, 23.0*
Phe 25	8.81	5.11	*2.67,*	H^δ 6.87; H^ε 7.00;	124.4	54.3	35.9	C^δ 131.0; C^ε 130.5;

			3.26	H^{ζ} 6.95				C^{ζ} 130.6
Ala 26	8.42	3.77	1.5		128.7	54.2	18.6	
Asp 27	9.05	4.24	2.84, 2.72		114.1	55.2	38.9	
Lys 28	7.53	4.56	1.77	H^{γ} 1.38; H^{δ} 1.56, 1.41; H^{ε} 2.82	117.8	56.2	35.9	C^{γ} 24.8; C^{δ} 28.4; C^{ε} 41.7
Val 29	8.35	4.45	2.57	H^{γ} *0.99*, *1.30*	114.2	58	31.7	C^{γ} *25.2, 20.6*
Pro 30		4.39	*1.96*, *2.61*	H^{γ} 2.06, 2.10; H^{δ} 3.54, 3.09		66.1	31.3	C^{γ} 27.2; C^{δ} 50.4
Lys 31	10.64	4	1.69, 1.54	H^{γ} 1.11, 0.89; H^{δ} 1.41, 1.31; H^{ε} 2.06, 1.85	123.5	60.2	32.3	C^{γ} 26.4; C^{δ} 29.5; C^{ε} 40.8
Thr 32	10.25	3.98	4.16	$H^{\gamma 2}$ 0.92; $H^{\gamma 1}$ 7.76	123.7	67.3	68.4	C^{γ} 22.2
Ala 33	9.27	4.03	1.43		125.4	55.8	18.2	
Glu 34	8.02	4.51	*2.26*, *1.75*	H^{γ} 2.45, 2.03	117	57.8	28	C^{γ} 33.5
Asn 35	7.12	4.05	*2.40*, *2.93*	$H^{\delta 2}$ 8.98, 6.80	115.4	56.6	39.4	$N^{\delta 2}$ 115.0
Phe 36	7	4.11	*3.05*, *2.95*	H^{δ} 6.42; H^{ε} 5.56	117.6	61.4	40	C^{ε} 130.7
Arg 37	8.93	3.63	1.93, 1.83	H^{γ} 1.50, 1.01; H^{δ} 3.53, 2.81; H^{ε} 8.89	120.8	60.3	29.9	C^{γ} 45.2; C^{δ} 41.0; N^{ε} 79.0
Ala 38	8.68	4.07	1.24		118.9	54.3	18.2	
Leu 39	8.15	3.74	*1.36*, *–0.33*	H^{γ} 1.75; H^{δ} *0.87*, *0.53*	120.5	57.1	40.9	C^{γ} 26.2; C^{δ} *26.7, 24.2*
Ser 40	7.88	4.44	4.22, 3.52	H^{γ} 3.43	119	62.3	62.8	
Thr 41	7.97	4.28	4.47	$H^{\gamma 2}$ 1.32; $H^{\gamma 1}$ 6.68	108.2	62.7	69.2	C^{γ} 22.4
Gly 42	7.57	3.86, 3.48			108.1	45.6		
Glu 43	8	4.11	*2.20*, *2.04*	H^{γ} 2.13, 1.79	118.5	58.4	29.9	C^{γ} 35.2
Lys 44	9.08	4.27	1.61, 0.89	H^{γ} 1.03; H^{δ} 1.44; H^{ε} 2.82, 2.67	118.1	54.1	30.3	C^{γ} 24.8; C^{δ} 27.3; C^{ε} 41.9
Gly 45	7.92	4.29, 3.54			105.3	44.4		
Phe 46	6.41	4.62	3.11, 2.71	H^{δ} 6.61; H^{ε} 6.98; H^{ζ} 7.06	113.5	53.9	39.4	C^{δ} 132.7; C^{ε} 130.6; C^{ζ} 129.2
Gly 47	7.72	4.34, 2.52			104.4	45.3		
Tyr 48	6.9	4.21	2.82, 2.64	H^{δ} 6.75; H^{ε} 6.13	113.5	57.1	38.4	
Lys 49	8.46	3.59	1.98, 1.59	H^{γ} 1.31, 1.24; H^{δ} 1.93, 1.76; H^{ε} 3.23, 3.05	124.6	60.9	31.2	C^{γ} 25.3; C^{δ} 29.7; C^{ε} 41.8
Gly 50	9.47	4.39, 3.69			117.6	45		
Ser 51	8.38	4.66	4.31, 4.19	H^{γ} 4.89	116.2	58.7	64.6	
Cys 52	9.86	5.89	3.03		114.8	56	31.7	
Phe 53	8.68	4.85	*2.89*, *2.63*	H^{δ} 6.89; H^{ε} 7.18;	122.8	58.1	38.7	C^{δ} 131.4; C^{ε} 130.8;

				H^{ζ} 7.36				C^{ζ} 128.2
His 54	7.62	4.71	3.27, 2.81	$H^{\delta 2}$ 6.84; $H^{\varepsilon 1}$ 7.35	119.9	57	31.3	$C^{\delta 2}$ 118.2; $C^{\varepsilon 1}$ 137.5
Arg 55	7.04	5.1	1.38, 1.25	H^{γ} 1.56, 1.21; H^{δ} 3.16, 3.12; H^{ε} 7.11	122.8	54.7	33.7	C^{γ} 28.0; C^{δ} 43.4; N^{ε} 83.9
Ile 56	9.15	4.59	1.57	$H^{\gamma 1}$ 1.55, 0.97; $H^{\gamma 2}$ 1.00; H^{δ} 0.85	126.2	61.5	41.6	$C^{\gamma 1}$ 27.1; $C^{\gamma 2}$ 17.6; $C^{\delta 1}$ 14.4
Ile 57	8.71	5.19	1.9	$H^{\gamma 1}$ 1.45, 1.14; $H^{\gamma 2}$ 1.11; H^{δ} 0.91	127.7	57.5	40	$C^{\gamma 1}$ 27.2; $C^{\gamma 2}$ 17.5; $C^{\delta 1}$ 13.4
Pro 58		4.32	*1.80*, *2.19*	H^{γ} 2.03, 1.86; H^{δ} 4.00, 3.44		62.9	31.9	C^{γ} 26.9; C^{δ} 52.1
Gly 59	9.68	4.03, 3.79			113.9	44.9		
Phe 60	8.15	5.08	3.15, 3.03	H^{δ} 7.26; H^{ε} 7.14	119	56.7	39.6	C^{δ} 130.3; C^{ε} 131.2
Met 61	8.08	5.31	*1.39*, *2.14*	H^{γ} 1.00; H^{ε} 1.25	111	54.8	34.7	C^{γ} 28.9; C^{ε} 18.3
Cys 62	8.45	4.87	2.96, 2.48	H^{γ} 1.60	114.6	57.3	30	
Gln 63	9.64	5.38	2.15, 1.79	H^{γ} 2.53, 1.98; $H^{\varepsilon 2}$ 6.96, 6.96	126.5	54.4	30.4	C^{γ} 33.1; $N^{\varepsilon 2}$ 109.1
Gly 64	7.36	4.71, 2.57			110.5	44.4		
Gly 65	9.29	*3.78*, *4.77*			105.6	46.4		
Asp 66	9.91	4.29	2.93, 1.70		123.7	51.5	38.7	
Phe 67	6.62	4.6	3.92, 2.57	H^{δ} 7.18; H^{ε} 7.32; H^{ζ} 7.41	115.9	55.8	39.3	C^{δ} 132.3; C^{ε} 131.7; C^{ζ} 128.5
Thr 68	7.32	4.64	4.09	$H^{\gamma 2}$ 0.68	108.9	61.6	68.7	C^{γ} 22.8
Arg 69	8.65	4.35	*1.87*, *1.60*	H^{γ} 1.46, 1.37; H^{δ} 3.05, 2.94; H^{ε} 7.01	121.8	55	31.6	C^{γ} 26.5; C^{δ} 42.7; N^{ε} 84.4
His 70[b]	6.64	4.39	3.22	$H^{\delta 2}$ 6.65; $H^{\varepsilon 1}$ 7.68	111	57.1	28.4	$C^{\delta 2}$ 118.0; $C^{\varepsilon 1}$ 138.1
Asn 71	7.52	4.59	3.14, 2.65	$H^{\delta 2}$ 7.63, 6.78	112.3	52.2	38.7	$N^{\delta 2}$ 110.3
Gly 72	9.62	4.40, 3.16			110.2	44.6		
Thr 73	7.91	4.48	4.25	$H^{\gamma 2}$ 1.02; $H^{\gamma 1}$ 5.77	111.8	62.1	70.3	C^{γ} 20.8
Gly 74	8.67	4.46, 3.46			113.7	44.8		
Gly 75	8.07	4.55, 2.54			108.8	43		
Lys 76	6.98	4.59	*1.54*, *1.88*	H^{γ} 0.98, 0.91; H^{δ} 1.19; H^{ε} 2.17, 1.53	115.5	55.7	34.5	C^{γ} 23.3; C^{δ} 29.2; C^{ε} 41.0
Ser 77	7.76	5.18	4.25	H^{γ} 5.10	114.1	56.8	69.1	
Ile 78	8.53	4.17	1.7	$H^{\gamma 1}$ 0.64, –0.47; $H^{\gamma 2}$ 0.71; H^{δ} 0.47	111	63.5	37.3	$C^{\gamma 1}$ 23.0; $C^{\gamma 2}$ 17.5; $C^{\delta 1}$ 14.1
Tyr 79	8.01	4.67	*2.33*, *3.42*	H^{δ} 6.41; H^{ε} 6.08	120.5	56.1	38.6	C^{δ} 132.5; C^{ε} 117.7
Gly 80	7.11	4.60,			106.4	43.8		

		3.79						
Glu 81	8.88	3.96	2.07	H^{γ} 2.34, 2.23	122.8	60.1	30.1	C^{γ} 36.3
Lys 82	7.84	5.51	1.63, 1.56	H^{γ} 1.25; H^{δ} 1.51, 1.55; H^{ε} 2.90	112.6	53.7	36.3	C^{γ} 24.3; C^{δ} 29.0; C^{ε} 42.0
Phe 83	9.16	4.95	3.02	H^{δ} 7.33; H^{ε} 7.51; H^{ζ} 7.38	116.4	55.7	41.3	C^{δ} 134.2; C^{ε} 130.8; C^{ζ} 128.5
Glu 84	9.25	3.8	2.02, 1.82	H^{γ} 2.28, 2.04	119.4	56.2	29.1	C^{γ} 35.2
Asp 85	8.57	4.23	2.40, 1.91		118.6	54.1	40.8	
Glu 86	9.44	3.79	2.12, 1.83	H^{γ} 2.36	131.5	60.2	31.6	C^{γ} 35.1
Asn 87	7.03	4.13	*2.73, 3.44*	$H^{\delta 2}$ 7.93, 6.88	106.5	52.6	39.3	$N^{\delta 2}$ 116.7
Phe 88	8.31	5.93	3.52, 2.53	H^{δ} 7.25; H^{ε} 6.86; H^{ζ} 6.85	112.7	55.7	38.7	C^{δ} 131.9; C^{ε} 130.6; C^{ζ} 128.7
Ile 89	8.27	3.65	1.54	$H^{\gamma 1}$ 1.48, 1.14; $H^{\gamma 2}$ 0.84; H^{δ} 0.90	119.6	64.8	38.9	$C^{\gamma 1}$ 29.2; $C^{\gamma 2}$ 16.8; $C^{\delta 1}$ 13.6
Leu 90	7.73	4.45	*1.82, 1.36*	H^{γ} 1.45; H^{δ} *0.75, 0.64*	117	53.9	41.8	C^{γ} 27.0; C^{δ} *26.8, 22.5*
Lys 91	8.05	4.63	*1.54, 2.26*	H^{γ} 1.44, 1.34; H^{δ} 1.62, 1.56; H^{ε} 3.00	118.7	54.3	34.5	C^{γ} 25.7; C^{δ} 28.1; C^{ε} 42.3
His 92	10.67	4.34	*2.88, 3.14*	$H^{\delta 1}$ 12.21; $H^{\delta 2}$ 6.74; $H^{\varepsilon 1}$ 8.05	122.2	56.8	25.9	$C^{\delta 2}$ 118.2; $C^{\varepsilon 1}$ 139.7; $N^{\delta 1}$ 169.1
Thr 93	7.25	4	4.43	$H^{\gamma 2}$ 1.20	110.2	63	69.3	C^{γ} 22.5
Gly 94	7.47	4.36, 3.64			107	45.4		
Pro 95		3.81	*1.84, 2.01*	H^{γ} 2.12, 1.83; H^{δ} 3.60, 3.39		62.5	32	C^{γ} 27.3; C^{δ} 49.6
Gly 96	9.25	4.56, 3.33			109.9	44.8		
Ile 97	6.76	4.11	2.22	$H^{\gamma 1}$ 1.80, 1.64; $H^{\gamma 2}$ 0.98; H^{δ} 0.96	121.2	59.3	37.8	$C^{\gamma 1}$ 28.9; $C^{\gamma 2}$ 20.2; $C^{\delta 1}$ 9.0
Leu 98	7.87	5	*0.15, 0.08*	H^{γ} 0.41; H^{δ} *–0.17, –0.59*	128.5	53.2	43.5	C^{γ} 26.4; C^{δ} *24.1, 25.1*
Ser 99	8.29	5.32	3.23, 2.88		118.3	54.9	65.3	
Met 100	8.55	5.26	2.57, 2.29	H^{γ} 2.79, 2.43; H^{ε} 2.08	122.8	53.7	31	C^{γ} 32.0; C^{ε} 16.1
Ala 101	8.03	4.26	1.1		126	51.4	19.4	
Asn 102	8.14	4.57	3.24, 2.89	$H^{\delta 2}$ 7.89, 6.16	113.2	53.8	40.4	$N^{\delta 2}$ 119.4
Ala 103	8.77	4.78	1.3		123.1	50.2	19	
Gly 104	8.11	4.59, 3.70			108.9	43.3		
Pro 105		4.32	*1.80, 2.32*	H^{γ} 2.11, 1.95; H^{δ} 3.60, 3.51		63.8	31.9	C^{γ} 27.6; C^{δ} 49.2
Asn 106	8.86	3.99	*3.08, 2.66*	$H^{\delta 2}$ 7.72, 7.08	118.9	54	36.9	$N^{\delta 2}$ 116.0
Thr 107	10.16	4.43	4.38	$H^{\gamma 2}$ 0.88; $H^{\gamma 1}$ 4.68	110	60	68.8	C^{γ} 21.0
Asn 108	7.37	4.21	1.54, 0.92	$H^{\delta 2}$ 7.41, 5.76	120.3	55.4	39.6	$N^{\delta 2}$ 112.7

Gly 109	9.14	4.59, 3.62			110.6	45.5		
Ser 110	8.74	4.7	4.60, 4.37	H^{γ} 4.93	116.8	57.5	66	
Gln 111	8.39	5.17	2.20, 2.07	H^{γ} 2.44, 1.84; $H^{\varepsilon 2}$ 7.30, 6.19	124.3	57.5	31.6	C^{γ} 35.2; $N^{\varepsilon 2}$ 111.0
Phe 112	8.06	5.7	3.28	H^{δ} 6.90, 7.80; H^{ε} 6.19, 7.22; H^{ζ} 6.75	117.6	55.4	43	C^{δ} 133.9
Phe 113	9.79	5.66	2.89, 2.83	H^{δ} 6.82; H^{ε} 6.75; H^{ζ} 6.88	116.2	54.3	42.6	C^{δ} 131.6; C^{ε} 130.4; C^{ζ} 129.3
Ile 114	9.1	4.79	1.8	$H^{\gamma 1}$ 2.09, 1.09; $H^{\gamma 2}$ 0.83; H^{δ} 1.20	118.4	60.1	40.1	$C^{\gamma 1}$ 27.2; $C^{\gamma 2}$ 17.7; $C^{\delta 1}$ 15.0
Cys 115	9.59	4.75	*3.09, 3.45*		125.3	60.7	28.5	
Thr 116	8.93	4.32	4.42	$H^{\gamma 2}$ 0.82	115.5	60.6	66.5	C^{γ} 23.0
Ala 117	7.6	4.36	1.41		122	50.4	22.6	
Lys 118	8.66	3.78	1.96, 1.63	H^{γ} 1.50; H^{δ} 1.74; H^{ε} 3.01	119.6	57.7	32.5	C^{γ} 24.6; C^{δ} 29.5; C^{ε} 41.7
Thr 119	7.31	3.62	2.81	$H^{\gamma 2}$ 0.97; $H^{\gamma 1}$ 3.07	118.8	57	68.5	C^{γ} 19.7
Glu 120	9.09	4.11	*2.18, 2.11*	H^{γ} 2.50, 2.39	124.4	59.1	29	C^{γ} 35.3
Trp 121	7.24	4.65	*3.37, 3.32*	$H^{\delta 1}$ 7.02; $H^{\varepsilon 1}$ 9.65; $H^{\varepsilon 3}$ 7.66; $H^{\zeta 3}$ 7.32; $H^{\eta 2}$ 7.11; $H^{\zeta 2}$ 6.61	117.5	59.5	26.8	$C^{\delta 1}$ 127.7; $C^{\varepsilon 3}$ 119.0; $C^{\zeta 2}$ 114.9; $C^{\zeta 3}$ 123.7; $C^{\eta 2}$ 125.1; $N^{\varepsilon 1}$ 129.8
Leu 122	6.99	4.24	*0.10, 1.13*	H^{γ} 0.37; H^{δ} *0.37, 0.65*	119.5	54.5	38.9	C^{γ} 26.0; C^{δ} *25.2, 21.5*
Asp 123	7.6	5.16	2.93, 2.68		121.8	55.6	39.3	
Gly 124	9.49	3.89, 2.88			110.8	44.8		
Lys 125	7.68	4.11	1.82, 1.67	H^{γ} 1.25, 1.22; H^{δ} 1.67; H^{ε} 3.00	115	56.1	35.4	C^{γ} 25.1; C^{δ} 29.0; C^{ε} 42.0
His 126	7.58	4.8	*3.18, 3.99*	$H^{\delta 2}$ 6.95; $H^{\varepsilon 1}$ 8.22	119.2	54.6	31.5	$C^{\delta 2}$ 118.1
Val 127	8.47	4.26	2	H^{γ} *1.13, 1.02*	124.7	63.6	33.4	C^{γ} *20.9, 21.1*
Val 128	9.48	4.16	1.71	H^{γ} *0.93, 0.08*	132.8	62.9	31.4	C^{γ} *21.7, 19.9*
Phe 129	8.07	5.25	3.10, 2.49	H^{δ} 6.52, 7.48; H^{ε} 5.64, 6.81; H^{ζ} 6.43	117.5	55.9	42.4	C^{δ} 130.6; C^{ε} 131.2
Gly 130	7.29	3.16, 2.98			110.5	46.3		
Lys 131	8.35	5.2	1.82	H^{γ} 1.50, 1.04; H^{δ} 1.76, 1.68; H^{ε} 2.96	115.1	54.7	35.9	C^{γ} 24.0; C^{δ} 29.3; C^{ε} 42.0
Val 132	9.01	3.89	1.91	H^{γ} *0.59, 1.03*	123.8	63.9	32.5	C^{γ} *21.2, 22.9*
Lys 133	9.44	4.42	1.71, 1.63	H^{γ} 1.44, 1.30; H^{δ} 1.62; H^{ε} 2.95	131.3	56.7	33.8	C^{γ} 24.6; C^{δ} 29.4; C^{ε} 41.3
Glu 134	7.53	4.56	1.95, 1.85	H^{γ} 2.18, 2.14	118.2	55.1	32.7	C^{γ} 36.6
Gly 135	8.65	4.73, 3.98			107.8	45.8		

Met 136	8.82	4.44	*1.92*, *2.09*	H^{γ} 2.75, 2.59; H^{ε} 1.98	122.3	56.7	30	C^{γ} 32.7; C^{ε} 17.1
Asn 137	8.89	4.45	2.82, 2.76	$H^{\delta 2}$ 7.73, 7.00	114.2	55.9	35.8	$N^{\delta 2}$ 114.6
Ile 138	7.63	3.75	2.44	$H^{\gamma 1}$ 1.51, 1.27; $H^{\gamma 2}$ 0.63; H^{δ} 0.65	123.9	61.3	34.3	$C^{\gamma 1}$ 27.0; $C^{\gamma 2}$ 17.2; $C^{\delta 1}$ 9.1
Val 139	7.24	3.84	2.44	H^{γ} *0.80*, *1.02*	121.7	66	31	C^{γ} *22.1, 23.1*
Glu 140	8.27	4.04	2.06, 1.96	H^{γ} 2.40, 2.20	117.1	59.1	29.4	C^{γ} 36.8
Ala 141	7.49	4.06	1.58		120.8	54.7	18	
Met 142	8.25	3.93	*2.51*, *1.93*	H^{γ} *2.26*, *2.62*; H^{ε} 1.16	117.3	59.5	33.6	C^{γ} 31.1; C^{ε} 14.4
Glu 143	7.81	3.71	2.14, 1.95	H^{γ} *2.04*, *2.34*	116.1	59.1	30.3	C^{γ} 37.7
Arg 144	7.02	3.91	1.45, 1.36	H^{γ} 1.58, 1.46; H^{δ} 3.04; H^{ε} 7.10	114.4	57.4	29.3	C^{γ} 27.5; C^{δ} 43.1; N^{ε} 84.8
Phe 145	7.6	4.79	*2.90*, *3.53*	H^{δ} 7.30; H^{ε} 7.16; H^{ζ} 7.27	115.1	57.6	38.9	C^{δ} 131.6; C^{ε} 129.2; C^{ζ} 129.8
Gly 146	7.5	*4.61*, *3.62*			104.5	43.9		
Ser 147	8.18	4.75	4.15, 4.04		109.8	58	65.5	
Arg 148	8.8	4.16	1.92, 1.88	H^{γ} 1.74, 1.69; H^{δ} 3.22; H^{ε} 7.24	119.8	59.5	29.7	C^{γ} 26.9; C^{δ} 43.0; N^{ε} 83.8
Asn 149	7.84	4.84	3.16, 2.80	$H^{\delta 2}$ 7.53, 6.72	111.4	52.1	38.1	$N^{\delta 2}$ 110.0
Gly 150	8.03	4.10, 3.93			109.9	44.8		
Lys 151	7.5	4.41	1.87, 1.82	H^{γ} 1.53, 1.48; H^{δ} 1.77, 1.74; H^{ε} 3.05	119.6	57	32.3	C^{γ} 24.8; C^{δ} 28.8; C^{ε} 41.9
Thr 152	8.81	5.53	4.63	$H^{\gamma 2}$ 1.34; $H^{\gamma 1}$ 5.01	116.3	59.8	71.1	C^{γ} 22.1
Ser 153	9.39	4.45	4.14, 4.02		116.8	58.7	63.5	
Lys 154	7.52	4.53	1.41, 0.83	H^{γ} 1.42, 1.18; H^{δ} 1.44, 1.13; H^{ε} 2.98, 2.89	119.1	54.4	38.3	C^{γ} 26.2; C^{δ} 29.2; C^{ε} 42.3
Lys 155	8.78	4.31	*1.78*, *1.87*	H^{γ} 1.40, 1.31; H^{δ} 1.66; H^{ε} 2.92, 2.90	121.5	56.1	32	C^{γ} 24.8; C^{δ} 28.8; C^{ε} 41.5
Ile 156	9.57	5.09	2.34	$H^{\gamma 1}$ 1.48, 1.44; $H^{\gamma 2}$ 0.92; H^{δ} 0.64	134	59.2	36.8	$C^{\gamma 1}$ 26.7; $C^{\gamma 2}$ 19.0; $C^{\delta 1}$ 13.4
Thr 157	9.23	5.26	3.88	$H^{\gamma 2}$ 0.99	117	59.4	72.5	C^{γ} 22.4
Ile 158	8.57	4.24	1.67	$H^{\gamma 1}$ 1.41, 0.34; $H^{\gamma 2}$ 0.31; H^{δ} –0.14	121.5	60.8	36.8	$C^{\gamma 1}$ 28.3; $C^{\gamma 2}$ 18.3; $C^{\delta 1}$ 13.7
Ala 159	8.86	4.12	1.29		132.3	54	19	
Asp 160	8.06	4.89	2.96, 2.86		111.3	52.6	43.5	
Cys 161	8.59	4.54	3.22, 3.09		115.8	55.1	31.1	
Gly 162	6.83	3.89, 3.55			103.9	45.3		

Gln 163	9.04	5.07	1.96, 1.75	H^{γ} 2.57, 2.47; $H^{\varepsilon 2}$ 8.14, 7.16	120.7	54.8	30.6	C^{γ} 33.2; $N^{\varepsilon 2}$ 110.6
Leu 164	8.59	4.61	1.62	H^{γ} 1.65; H^{δ} *0.83, 0.74*	125.8	54.7	43.3	C^{γ} 27.1; C^{δ} *25.2, 23.2*
Glu 165	8.1	4.16	2.09, 1.92	H^{γ} 2.20	125.9	57.9	31.6	C^{γ} 36.8

Table S2. X-ray refinement statistics

Protein	CypA
Ligand	1
PDB ID	6GS6
Data collection and processing	
High resolution limit	1.16 (1.16)
Low resolution limit	54.57 (1.18)
Completeness	99.64 (99.27)
Multiplicity	9.1 (6.5)
I/sigma	14.2 (1.0)
Rmerge	0.048 (1.70)
Unit cell dimensions:	
a (Å)	63.01
b (Å)	63.01
c (Å)	94.72
α (°)	90.00
β (°)	90.00
γ (°)	120.00
Space group	P 3_2 2 1
Total observations	686777 (23855)
Total unique	75550 (3671)
Refinement statistics	
No. of residues per chain (No. of chains)	165
No. of ligands	1
No. of waters	83
Percentage of free reflections	5.20
R factor	0.15
R free	0.20
Rms BondLength	0.01
Rms BondAngle	1.43
Ramachandran plot	
Favoured (%)	96.7
Allowed (%)	3.3
No. of outliers*	0

Table S3. Exchange parameters for WT and D66A obtained from a two state exchange model.

WT		
Residue	**Δω**	**Err**
Glu 15	0.2	0.0
Leu 24	0.6	0.1
Thr 32	2.2	0.2
Phe 46	1.0	0.2
Tyr 48	1.1	0.2
Asp 66	3.0	0.2
Thr 68	6.3	0.1
His 70	1.1	0.2
Asn 71	5.9	0.2
Thr 73	1.3	0.2
Gly 74	5.9	0.2
Ser 77	3.9	0.2
Gly 80	1.0	0.2
Asn 87	1.1	0.2
Ile 89	1.4	0.2
Gly 96	1.4	0.2
Ser 99	1.8	0.2
Asn 102	1.9	0.2
Ser 110	3.0	0.2
Gln 111	1.8	0.2
Phe 113	1.4	0.2
Glu 120	1.4	0.2
Leu 122	1.4	0.2
Lys 131	1.4	0.2
$k_{ex}(s^{-1})$	2150	90
pb(frac)	0.021	0.001
D66A		
Residue	**Δω**	**Err**
Ala 33	2.5	0.3
Arg 55	0.8	0.3
Gly 72	2.4	0.2
Gly 74	-2.2	0.2
Gly 80	-7.6	0.2
Phe 83	3.8	0.2
Asn 87	2.2	0.2
Glu 120	3.9	0.1
kex(s^{-1})	2200	350
pb(frac)	0.007	0.001

Table S4. Measured Rex values for WT, D66A. The 70s-loop region is highlighted.

WT		D66A	
Residue	**(s^{-1})**	**Residue**	**(s^{-1})**
Met 1	ND	**Met 1**	ND
Val 2	ND	**Val 2**	0.0
Asn 3	ND	**Asn 3**	ND
Thr 5	0.2	**Thr 5**	0.4
Val 6	ND	**Val 6**	ND
Phe 7	ND	**Phe 7**	ND
Phe 8	ND	**Phe 8**	1.0
Asp 9	1.1	**Asp 9**	1.2
Ile 10	1.3	**Ile 10**	0.3
Ala 11	1.3	**Ala 11**	2.7
Val 12	ND	**Val 12**	ND
Asp 13	2.2	**Asp 13**	ND
Gly 14	2.7	**Gly 14**	0.7
Glu 15	1.6	**Glu 15**	1.0
Leu 17	ND	**Leu 17**	2.4
Gly 18	3.6	**Gly 18**	1.0
Arg 19	ND	**Arg 19**	1.3
Val 20	ND	**Val 20**	2.5
Ser 21	0.4	**Ser 21**	2.1
Phe 22	ND	**Phe 22**	ND
Glu 23	0.2	**Glu 23**	1.0
Leu 24	0.4	**Leu 24**	1.2
Phe 25	1.5	**Phe 25**	0.9
Ala 26	1.7	**Ala 26**	ND
Asp 27	ND	**Asp 27**	1.3
Lys 28	ND	**Lys 28**	ND
Val 29	2.0	**Val 29**	ND
Lys 31	2.3	**Lys 31**	1.2
Thr 32	2.1	**Thr 32**	ND
Ala 33	ND	**Ala 33**	1.3
Glu 34	ND	**Glu 34**	ND
Asn 35	ND	**Asn 35**	1.0
Phe 36	0.9	**Phe 36**	2.5
Arg 37	1.4	**Arg 37**	ND
Ala 38	0.1	**Ala 38**	0.4
Leu 39	ND	**Leu 39**	1.1
Ser 40	1.7	**Ser 40**	ND
Thr 41	0.6	**Thr 41**	0.5
Gly 42	1.3	**Gly 42**	2.7
Glu 43	0.9	**Glu 43**	ND
Lys 44	ND	**Lys 44**	ND

Gly 45	0.00	**Gly 45**	ND
Phe 46	1.3	**Phe 46**	0.7
Gly 47	2.0	**Gly 47**	4.7
Tyr 48	2.4	**Tyr 48**	1.1
Lys 49	0.6	**Lys 49**	0.1
Gly 50	ND	**Gly 50**	0.7
Ser 51	ND	**Ser 51**	ND
Cys 52	ND	**Cys 52**	1.4
Phe 53	0.5	**Phe 53**	2.7
His 54	4.0	**His 54**	7.2
Arg 55	3.4	**Arg 55**	3.7
Ile 56	0.6	**Ile 56**	ND
Ile 57	ND	**Ile 57**	3.2
Gly 59	0.0	**Gly 59**	ND
Phe 60	2.1	**Phe 60**	0.4
Met 61	ND	**Met 61**	ND
Cys 62	1.3	**Cys 62**	2.3
Gln 63	ND	**Gln 63**	0.0
Gly 64	ND	**Gly 64**	ND
Gly 65	ND	**Gly 65**	ND
Asp 66	13.4	**Ala 66**	0.9
Phe 67	ND	**Phe 67**	ND
Thr 68	18.4	**Thr 68**	ND
Arg 69	ND	**Arg 69**	ND
His 70	3.2	**His 70**	ND
Asn 71	24.5	**Asn 71**	ND
Gly 72	ND	**Gly 72**	2.9
Thr 73	2.3	**Thr 73**	ND
Gly 74	21.5	**Gly 74**	3.0
Gly 75	ND	**Gly 75**	ND
Lys 76	3.6	**Lys 76**	ND
Ser 77	10.7	**Ser 77**	3.9
Ile 78	1.2	**Ile 78**	ND
Tyr 79	2.7	**Tyr 79**	6.3
Gly 80	4.0	**Gly 80**	5.2
Glu 81	ND	**Glu 81**	ND
Lys 82	6.8	**Lys 82**	7.7
Phe 83	2.1	**Phe 83**	6.3
Glu 84	1.7	**Glu 84**	2.7
Asp 85	ND	**Asp 85**	2.0
Glu 86	ND	**Glu 86**	ND
Asn 87	4.0	**Asn 87**	2.0
Phe 88	ND	**Phe 88**	0.6
Ile 89	2.2	**Ile 89**	ND
Leu 90	ND	**Leu 90**	1.5
Lys 91	0.8	**Lys 91**	3.6

His 92	2.0	**His 92**	1.8
Thr 93	0.6	**Thr 93**	0.6
Gly 94	0.5	**Gly 94**	0.5
Gly 96	2.0	**Gly 96**	ND
Ile 97	2.1	**Ile 97**	3.2
Leu 98	3.3	**Leu 98**	ND
Ser 99	4.0	**Ser 99**	4.8
Met 100	1.0	**Met 100**	ND
Ala 101	ND	**Ala 101**	7.7
Asn 102	5.8	**Asn 102**	0.7
Ala 103	3.9	**Ala 103**	ND
Gly 104	2.2	**Gly 104**	0.4
Asn 106	ND	**Asn 106**	0.1
Thr 107	ND	**Thr 107**	1.3
Asn 108	ND	**Asn 108**	2.6
Gly 109	ND	**Gly 109**	1.2
Ser 110	5.5	**Ser 110**	ND
Gln 111	6.8	**Gln 111**	0.3
Phe 112	0.2	**Phe 112**	ND
Phe 113	4.6	**Phe 113**	2.6
Ile 114	0.8	**Ile 114**	0.3
Cys 115	0.3	**Cys 115**	0.5
Thr 116	ND	**Thr 116**	ND
Ala 117	3.1	**Ala 117**	ND
Lys 118	0.8	**Lys 118**	ND
Thr 119	ND	**Thr 119**	ND
Glu 120	1.6	**Glu 120**	4.4
Trp 121	ND	**Trp 121**	ND
Leu 122	1.8	**Leu 122**	1.5
Asp 123	ND	**Asp 123**	3.5
Gly 124	4.3	**Gly 124**	ND
Lys 125	1.8	**Lys 125**	0.5
His 126	ND	**His 126**	1.2
Val 127	0.6	**Val 127**	2.2
Val 128	0.8	**Val 128**	1.6
Phe 129	ND	**Phe 129**	ND
Gly 130	0.7	**Gly 130**	0.8
Lys 131	3.6	**Lys 131**	0.3
Val 132	ND	**Val 132**	2.2
Lys 133	ND	**Lys 133**	ND
Glu 134	ND	**Glu 134**	ND
Gly 135	1.3	**Gly 135**	ND
Met 136	ND	**Met 136**	ND
Asn 137	0.1	**Asn 137**	0.6
Ile 138	1.9	**Ile 138**	ND
Val 139	ND	**Val 139**	0.1

Glu 140	ND	**Glu 140**	1.7
Ala 141	ND	**Ala 141**	0.6
Met 142	ND	**Met 142**	ND
Glu 143	1.4	**Glu 143**	ND
Arg 144	0.1	**Arg 144**	ND
Phe 145	ND	**Phe 145**	0.1
Gly 146	1.6	**Gly 146**	1.9
Ser 147	0.8	**Ser 147**	1.3
Arg 148	1.0	**Arg 148**	ND
Asn 149	1.7	**Asn 149**	3.3
Gly 150	1.4	**Gly 150**	0.6
Lys 151	ND	**Lys 151**	0.0
Thr 152	0.0	**Thr 152**	1.6
Ser 153	ND	**Ser 153**	3.0
Lys 154	ND	**Lys 154**	0.3
Lys 155	1.4	**Lys 155**	ND
Ile 156	ND	**Ile 156**	2.3
Thr 157	0.2	**Thr 157**	1.1
Ile 158	4.1	**Ile 158**	ND
Ala 159	ND	**Ala 159**	ND
Asp 160	1.7	**Asp 160**	2.7
Cys 161	0.0	**Cys 161**	0.4
Gly 162	ND	**Gly 162**	1.3
Gln 163	ND	**Gln 163**	1.5
Leu 164	ND	**Leu 164**	0.5
Glu 165	ND	**Glu 165**	0.6

Available datasets

Dataset S1. 10000 representative structures of the MSM ensembles, states assignments and rate matrices for CypA, D66A, H70A CypA.

Dataset S2: Video summarizing the conformational changes in CypA

These datasets are available at https://bitbucket.org/jjuarez84/cypa-datasets/src